The NEXT experiment for $\beta\beta0\nu$ searches at LSC

A status report

The NEXT COLLABORATION

May 2013

Contents

Chapter 1

Introduction

In this report we present the current status of the *Neutrino Experiment with a Xenon TPC* (**NEXT**)[1]. The primary goal of the project is the construction, commissioning and operation of the NEXT-100 detector, a high-pressure, xenon (HPXe) Time Projection Chamber (TPC). NEXT-100 will search for neutrinoless double beta decay ($\beta\beta0\nu$) events in ^{136}Xe, using 100 kg of xenon enriched at 90% in the isotope ^{136}Xe. The experiment will operate at the Canfranc Underground Laboratory (LSC). If fully funded, the detector can be completed in 2014 and a physics run can start in 2015.

The discovery potential of NEXT is very large. It combines four desirable features that make it an almost-ideal experiment for $\beta\beta0\nu$ searches, namely:

1. Excellent energy resolution (better than 1% FWHM in the region of interest).
2. A topological signature (the observation of the tracks of the two electrons).
3. A fully active, very radiopure apparatus of large mass.
4. The capability of extending the technology to much larger masses.

Currently, two xenon-based experiments, with a mass in the range of hundred kilograms are dominating the field of $\beta\beta0\nu$ searches. These are: EXO-200 (a liquid xenon TPC) and KamLAND-Zen (a large, liquid scintillator calorimeter, where the xenon is dissolved in the scintillator). Compared with them, NEXT features much better resolution and the extra handle of the identification of the two electrons, which could result in a discovery, in spite of a late start. On the other hand, if evidence is found by EXO-200 or KamLAND-Zen of the existence of a signal, NEXT would be needed to confirm it in an unambiguous way, in particular given the discriminating power of the topological signature.

Recent cosmological studies hint that the effective neutrino mass could be in the range of 20 to 100 meV. This is barely accessible to the current generation of experiments, but within reach of apparatus deploying target masses in the range of one ton, provided that those new-generation experiments can, indeed, reduce the specific background rate in the

[1] `http://next.ific.uv.es/next`

same proportion that they increase their target mass. In that respect, the physics case of a HPXe TPC is outstanding, given the combination of excellent energy resolution and the high background rejection power that the observation of the two electrons provides. The NEXT-100 detector could, therefore, be the springboard for the next generation of $\beta\beta0\nu$ experiments.

The NEXT project is being carried out by the international NEXT collaboration, which includes institutions from Spain, Portugal, USA, Russia and Colombia. The leading institution is the *Instituto de Física Corpuscular (IFIC)*, a joint centre between the University of Valencia, and the Spanish national research institution, CSIC. The principal investigator at IFIC and spokesperson of NEXT is J.J. Gómez-Cadenas (PI hereafter). The technical coordinator and project manager (Dr. I. Liubarsky), the software coordinator (Dr. M. Sorel), and several other key coordinators and leading engineers, are also at IFIC.

The Other national institutions in NEXT are the UPV (Polytechnic University of Valencia) the UdG (University of Girona), UNIZAR (University of Zaragoza), UAM (U. Autnoma of Madrid) and USC (U. of Santiago de Compostela). UPV has designed the electronics and DAQ of the experiment, and coordinates (prof. F. Toledo) the production of the electronics cards for the energy and tracking plane, as well as the DAQ. In addition, the UPV, working closely with the UdG, has designed the mechanical infrastructures of the experiment and co-ordinates its construction (prof. J.L. Perez, prof. L. Ripoll). UNIZAR coordinates the radiopurity campaign (prof. S. Cebrin), and contributes also to the the experiment integration (Dr. T. Dafni) and to the R&D towards high-performance gas mixtures (Dr. I. Irastorza, Dr. D. Gonzlez). UAM contributes to the radiopurity campaign, coordinating in particular the studies related with PMT screening (Prof. L. Labarga). USC contributes to the physics studies of NEXT and the data analysis of NEXT prototype (Prof. J.A. Hernando).

Concerning the international contribution, the Lawrence Berkeley National Laboratory (LBNL), the Texas A&M University (TAMU) and Iowa State University (ISU), are playing a major role in the development of the project. The leader of the LBNL group is Dr. D. Nygren, the inventor of the TPC technology and one of the most prestigious physicists in the field. He has made seminal contributions to every aspect of NEXT. The leader of Texas A&M group is Prof. J. White, one of the best known world experts in HPXe technology. Prof. J. Hauptman from Iowa State is a well known and experienced physicist. A large source of expertise is also provided by the portuguese contribution. The Coimbra group, led by Prof. J.M.F. Dos Santos is one of the pioneers in the electroluminescent technology adopted by NEXT and works in collaboration with the group at U. of Aveiro (prof. J. Veloso). The technology of electroluminescence itself was invented by prof. C.A.N. Conde (together with prof. A.J.P.L. Policarpo) who is also a member of the collaboration. NEXT also includes the collaboration of UAN (University Antonio Nario), of Colombia and a group of JINR (Russia). UAN contributes to the physics studies and data analysis (Prof. R. Gutierrez) and JINR has been instrumental to acquire the enriched xenon gas.

The main source of funding in NEXT during the period 2009–2013 has been CUP

(Canfranc Undeground Physics) a 5 year, 5 M€ grant, which has supported the initial R&D needed to kick-start the project, the equipment of state-of-the-art laboratories in several Spanish institutions and the construction of prototypes, in particular NEXT-DEMO, a 5 kg demonstrator of NEXT, which is currently the largest HPXe chamber in the world. Funds from CUP have also been used to hire physicists, engineers and post-docs in the participating institutions. This is of particular relevance, given the high level of scientific expertise required by the project, and its rapid development.

Funds from CUP are also being invested in covering part of the construction costs of the NEXT-100 apparatus. Other sources of funding are: regular research projects granted by the Spanish science office (currently MINECO); contributions from the LSC itself, chiefly towards the infrastructures needed for the experiment; contributions from the international partners. All together, they finance a substantial part of the detector. However, to complete the construction of the NEXT-100 apparatus and to exploit it, additional funding is needed, as will be discussed in this report.

CUP was constituted as a consortium of national institutions, most of which are also part of NEXT. However, CUP also included a phenomenological activity, called CAFE (Canfranc Future Experiment).

While the CUP consortium has not changed since its beginning (in 2009), the NEXT collaboration has evolved significantly. The original document defining NEXT was the Letter of Intent (LOI) to the LSC scientific committee (LSC-SC hereafter), published in 2009, which was also the first year of CUP funding. In 2011, after two years of intense R&D, a Conceptual Design Report (CDR) defined the detector technological choices and also formalised the composition of the NEXT collaboration. A Technical Design Report (TDR) was published in preliminary form in late 2011 and in final form in 2012. After demonstrating the excellent performance of HPXe detectors using the large-scale prototypes NEXT-DEMO (IFIC) and NEXT-DBDM (LBNL), the collaboration is moving into the construction phase, with the goal of starting a physics run in 2015.

The project has evolved very satisfactorily, from the initial LOI in 2009 to the TDR in 2012. A substantial number of papers, proceeding reports and conferences, documenting and demonstrating the physics case, the results of the prototypes and the technological choices can be found in the NEXT web page: `http://next.ific.uv.es/next/talks.html`.

This report is organised in two parts.

- Part one describes the physics of NEXT, the detector design, the EL prototypes and the results that demonstrate the technological choices and discovery potential.
- Part two describes the managerial and financial aspects of the NEXT project.

Part I

Physics and detector

Chapter 2

The physics of NEXT

2.1 Majorana neutrinos and $\beta\beta0\nu$ experiments

Neutrinos, unlike the other Standard Model fermions, could be Majorana particles, that is, indistinguishable from their antiparticles, since they are chargeless. The existence of Majorana neutrinos would have decisive implications in particle physics and cosmology. If neutrinos are Majorana particles, there must exist a new scale of physics, the level of which is inversely proportional to neutrino masses, that characterises new underlying dynamics beyond the Standard Model. The existence of such a new scale provides the simplest explanation of why neutrino masses are so much lighter than the charged fermions. Understanding the new physics that underlies neutrino masses is one of the most important open questions in particle physics. It could have profound implications in our understanding of the mechanism of symmetry breaking, the origin of mass and the flavour problem [1].

Furthermore, the existence of Majorana neutrinos would imply that lepton number is not a conserved quantum number which could be the origin of the matter-antimatter asymmetry observed in the Universe. The new physics related to neutrino masses could provide a new mechanism to generate the asymmetry, called leptogenesis. Although the predictions are model dependent, two essential ingredients must be confirmed experimentally: 1) the violation of lepton number and 2) CP violation in the lepton sector.

The only practical way to establish experimentally that neutrinos are their own antiparticle is the detection of neutrinoless double beta decay ($\beta\beta0\nu$). This is a postulated very slow radioactive process in which a nucleus with Z protons decays into a nucleus with $Z + 2$ protons and the same mass number A, emitting two electrons that carry essentially all the energy released ($Q_{\beta\beta}$). The process can occur if and only if neutrinos are massive, Majorana particles.

Several underlying mechanisms — involving, in general, physics beyond the Standard Model — have been proposed for $\beta\beta0\nu$, the simplest one being the virtual exchange of light Majorana neutrinos. Assuming this to be the dominant process at low energies, the half-life of $\beta\beta0\nu$ can be written as:

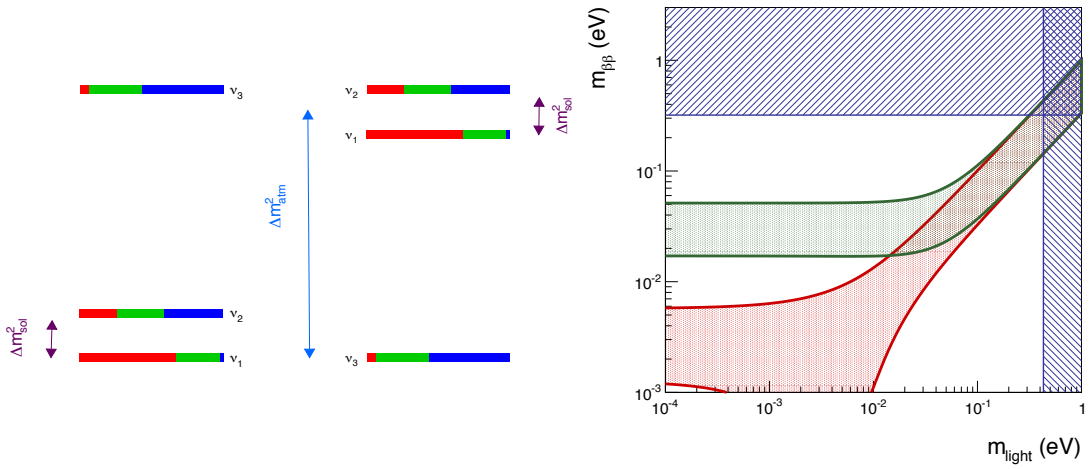

Figure 2.1: The left panel shows the normal (left) and inverted (right) mass orderings. The electron, muon and tau flavor content of each neutrino mass eigenstate is shown via the red, green and blue fractions, respectively. The right panel shows the effective neutrino Majorana mass, $m_{\beta\beta}$, as a function of the lightest neutrino mass, m_{light}. The green band corresponds to the inverse hierarchy of neutrino masses, whereas the red corresponds to the normal ordering. The upper bound on the lightest neutrino mass comes from cosmological bounds; the bound on the effective Majorana mass from $\beta\beta0\nu$ constraints.

$$(T^{0\nu}_{1/2})^{-1} = G^{0\nu} \left|M^{0\nu}\right|^2 m^2_{\beta\beta}\,. \tag{2.1}$$

In this equation, $G^{0\nu}$ is an exactly-calculable phase-space integral for the emission of two electrons; $M^{0\nu}$ is the nuclear matrix element (NME) of the transition, which has to be evaluated theoretically; and $m_{\beta\beta}$ is the *effective Majorana mass* of the electron neutrino:

$$m_{\beta\beta} = \left| \sum_i U^2_{ei}\ m_i \right|, \tag{2.2}$$

where m_i are the neutrino mass eigenstates and U_{ei} are elements of the neutrino mixing matrix. Therefore, a measurement of the decay rate of $\beta\beta0\nu$ would provide direct information on neutrino masses.

The relationship between $m_{\beta\beta}$ and the actual neutrino masses m_i is affected by the uncertainties in the measured oscillation parameters, the unknown neutrino mass ordering (normal or inverted), and the unknown phases in the neutrino mixing matrix (both Dirac and Majorana). The current knowledge on neutrino masses and mixings provided by neutrino oscillation experiments is summarized in the left panel of Figure 2.1. The diagram shows the two possible mass orderings that are compatible with neutrino oscillation data, with increasing neutrino masses from bottom to top. The relationship between $m_{\beta\beta}$ and the lightest neutrino mass m_{light} (which is equal to m_1 or m_3 in the

normal and inverted mass orderings, respectively) is illustrated in the right panel of Figure 2.1.

The upper bound on the effective Majorana mass corresponds to the experimental constraint set by the Heidelberg-Moscow (HM) experiment, which was until very recently the most sensitive limit to the half-life of $\beta\beta0\nu$: $T^{0\nu}_{1/2}(^{76}\mathrm{Ge}) \geq 1.9 \times 10^{25}$ years at 90% CL [2]. A subgroup of the HM experiment interpreted the data as *evidence* of a positive signal, with a best value for the half-life of 1.5×10^{25} years, corresponding to an effective Majorana mass of about 400 meV [3]. This claim was very controversial and the experimental effort of the last decade has been focused in confirming or refuting it. The recent results from the KamLAND-ZEN and EXO experiments (both of them based in xenon, like NEXT) have almost excluded the claim, and new data from other experiments such as GERDA, Majorana and CUORE will definitively settle the question in the next two years.

2.2 The current generation of $\beta\beta0\nu$ experiments

The detectors used to search for $\beta\beta0\nu$ are designed, in general, to measure the energy of the radiation emitted by a $\beta\beta0\nu$ source. In a neutrinoless double beta decay, the sum of the kinetic energies of the two released electrons is always the same, and equal to the mass difference between the parent and the daughter nuclei: $Q_{\beta\beta} \equiv M(Z, A) - M(Z + 2, A)$. However, due to the finite energy resolution of any detector, $\beta\beta0\nu$ events would be reconstructed within a given energy range centred around $Q_{\beta\beta}$ and typically following a gaussian distribution. Other processes occurring in the detector can fall in that region of energies, thus becoming a background and compromising drastically the sensitivity of the experiment [4].

All double beta decay experiments have to deal with an intrinsic background, the standard two-neutrino double beta decay ($\beta\beta2\nu$), that can only be suppressed by means of good energy resolution. Backgrounds of cosmogenic origin force the underground operation of the detectors. Natural radioactivity emanating from the detector materials and surroundings can easily overwhelm the signal peak, and hence careful selection of radiopure materials is essential. Additional experimental signatures, such as event topological information, that allow the distinction of signal and background, are a bonus to provide a robust result.

Besides energy resolution and control of backgrounds, several other factors such as detection efficiency and scalability to large masses must be taken into consideration in the design of a double beta decay experiment. The simultaneous optimisation of all these parameters is most of the time conflicting, if not impossible, and consequently many different experimental techniques have been proposed. In order to compare them, a figure of merit, the experimental sensitivity to $m_{\beta\beta}$, is normally used [4]:

$$m_{\beta\beta} \propto \sqrt{1/\varepsilon} \left(\frac{b\ \delta E}{M\ t} \right)^{1/4}, \tag{2.3}$$

where ε is the signal detection efficiency, M is the $\beta\beta$ isotope mass used in the experiment,

t is the data-taking time, δE is the energy resolution and b is the background rate in the region of interest around $Q_{\beta\beta}$ (expressed in counts per kg of $\beta\beta$ isotope, year and keV).

The status of the field has been the subject of several recent reviews [5–8]. Among the on-going and planned experiments, many different experimental techniques are utilised, each with its pros and cons. The time–honored approach of emphasising energy resolution and detection efficiency is currently spearhead by germanium calorimeters like GERDA [9] and MAJORANA [10], as well as tellurium bolometers such as CUORE [11].

A different and powerful approach proposes the use of xenon-based experiments. Two of them, EXO-200 [12] and KamLAND-Zen [13] are already operating, while NEXT [14] is in the initial stages of construction, and foresees to start taking data in 2015.

Other experiments that will operate in the next few years are the SuperNEMO demonstrator [7], a tracker-calorimeter approach which provides a powerful topological signal (the observation of the two electrons emitted in a $\beta\beta$ decay) but is hard to extrapolate to larger masses (the demonstrator itself will have a mass of less than 10 kg of isotope), and SNO+ [5], a large liquid scintillator calorimeter (the same approach as KamLAND-Zen), in which natural Neodymium is dissolved in the scintillator. Neodymium is a very interesting isotope, whose large $Q_{\beta\beta}$ suppresses many of the low-energy background than other experiments have to deal with, but the $\beta\beta0\nu$ decaying isotope, ^{150}Nd is only 5% of the natural Neodymium, limiting the total mass that the experiment can deploy.

2.3 Other xenon experiments

Xenon is an almost-optimal element for $\beta\beta0\nu$ searches, featuring many desirable properties, both as a source and as a detector. It has two naturally-occurring isotopes that can decay via the $\beta\beta$ process, ^{134}Xe ($Q_{\beta\beta} = 825$ keV) and ^{136}Xe ($Q_{\beta\beta} = 2458$ keV). The latter, having a higher Q value, is preferred since the decay rate is proportional to $Q^5_{\beta\beta}$ and the radioactive backgrounds are less abundant at higher energies. Moreover, the $\beta\beta2\nu$ mode of ^{136}Xe is slow ($\sim 2.3 \times 10^{21}$ years [15, 16]) and hence the experimental requirement for good energy resolution to suppress this particular background is less stringent than for other $\beta\beta$ sources. The process of isotopic enrichment in the isotope ^{136}Xe is relatively simple and cheap compared to that of other $\beta\beta$ isotopes. Xenon has no long-lived radioactive isotopes and is therefore intrinsically clean.

As a detector, xenon is a noble gas, therefore one can build a time projection chamber (TPC) with pure xenon as detection medium. Both a liquid xenon (LXe) TPC and a (high-pressure) gas (HPXe) TPC are suitable technologies, chosen by the EXO-200 and the NEXT experiment respectively. Nevertheless, energy resolution is much better in gas than in liquid, since, in its gaseous phase, xenon is characterized by a small Fano factor, meaning that the fluctuations in the ionization production have a sub-poissonian behaviour. Being a noble gas, xenon can also be dissolved in liquid scintillator. This is the approach of the KamLAND-Zen experiment.

2.3.1 KamLAND-Zen

The KamLAND-Zen experiment is a modification of the well-known KamLAND neutrino detector [17]. A transparent balloon, with a $\sim$ 3 m diameter, containing 13 tons of liquid scintillator loaded with 320 kg of xenon (enriched to 91% in ^{136}Xe) is suspended at the centre of KamLAND. The scintillation light generated by events occurring in the detector is recorded by an array of photomultipliers surrounding it. From the detected light pattern, the position of the event vertex is reconstructed with a spatial resolution of about 15 cm/$\sqrt{E(\mathrm{MeV})}$. The energy resolution is $(6.6 \pm 0.3)\%/\sqrt{E(\mathrm{MeV})}$, that is, 9.9% FWHM at the Q value of ^{136}Xe. The signal detection efficiency is ~ 0.42 due to the tight fiducial cut introduced to reject backgrounds originating in the balloon. The achieved background rate in the energy window between 2.2 MeV and 3.0 MeV is 10^{-3} counts/(keV $\cdot$ kg $\cdot$ y).

KamLAND-Zen has searched for $\beta\beta0\nu$ events with an exposure of 89.5 kg·year. They have published a limit on the half-life of $\beta\beta0\nu$ of $T^{0\nu}_{1/2}(^{136}\mathrm{Xe}) > 1.9 \times 10^{25}$ years [18].

2.3.2 EXO

The EXO-200 detector [12] is a symmetric LXe TPC deploying 110 kg of xenon (enriched to 80.6% in ^{136}Xe).

In EXO-200, ionisation charges created in the xenon by charged particles drift under the influence of an electric field towards the two ends of the chamber. There, the charge is collected by a pair of crossed wire planes which measure its amplitude and transverse coordinates. Each end of the chamber includes also an array of avalanche photodiodes (APDs) to detect the 178-nm scintillation light. The sides of the chamber are covered with teflon sheets that act as VUV reflectors, improving the light collection. The simultaneous measurement of both the ionisation charge and scintillation light of the event may in principle allow to reach a detector energy resolution as low as 3.3% FWHM at the ^{136}Xe Q value, for a sufficiently intense drift electric field [19].

The EXO-200 detector achieves currently an energy resolution of 4% FWHM at $Q_{\beta\beta}$, and a background rate measured in the *region of interest* (ROI) of 1.5×10^{-3} counts/(keV $\cdot$ kg $\cdot$ y). The experiment has also searched for $\beta\beta0\nu$ events. The total exposure used for the published result is 32.5 kg·year. They have published a limit on the half-life of $\beta\beta0\nu$ of $T^{0\nu}_{1/2}(^{136}\mathrm{Xe}) > 1.6 \times 10^{25}$ years [20].

The combination of the KamLAND-Zen and EXO results yields a limit $T^{0\nu}_{1/2}(^{136}\mathrm{Xe}) > 3.4 \times 10^{25}$ years [18], which essentially excludes the long-standing claim of Klapdor-Kleingrothaus and collaborators [21].

2.4 The NEXT experiment and its innovative concepts: a preview

The NEXT experiment will search for $\beta\beta0\nu$ in ^{136}Xe using a high-pressure xenon gas (HPXe) time projection chamber (TPC) containing 100 kilogram of enriched gas, and

called NEXT-100. Such a detector offers major advantages for the search of neutrinoless double beta decay, namely:

- **Excellent energy resolution**, with an intrinsic limit of about 0.3% FWHM at $Q_{\beta\beta}$ and 0.5% demonstrated by our prototypes. For reference, the best energy resolution in the field is achieved by germanium experiments, such as GERDA and MAJORANA, or bolometers such as CUORE, with typical resolutions in the range of 0.2% FWHM at $Q_{\beta\beta}$. NEXT-100 targets a resolution which is a factor two worse than these, but a factor 8 (20) better than that of EXO (KamLAND-Zen), the other xenon experiments.

- **Tracking capabilities** that provide a powerful topological signature to discriminate between signal (two electron tracks with a common vertex) and background (mostly, single electrons). The topological signature results in an expected background rate of the order of 5×10^{-4} counts/(keV $\cdot$ kg $\cdot$ y), improving EXO and KamLAND-Zen by a factor two, and the germanium calorimeters and tellurium bolometers by a factor five to ten.

- **A fully active and homogeneous detector**, with no dead regions. Since 3-dimensional reconstruction is possible, events can be located in a fiducial region away from surfaces, where most of the background arises. This is a common feature with the two other xenon experiments.

- **Scalability** of the technique to larger masses, thanks to the fact that: a) xenon is noble gas, suitable for detection and with no intrinsic radioactivity; b) enriched xenon (in Xe-136) can be procured at a moderately limited cost, for instance a factor 10 cheaper than the baseline Ge-76 choice. This is also a common feature with the other two xenon experiments.

2.5 Discovery potential

Recently, an upper limit for the sum of the three light neutrino masses has been reported by Planck measurements of the cosmic microwave background (CMB) [22, 23]:

$$\sum m_\nu = m_1 + m_2 + m_3 < 0.230 \text{ eV}. \tag{2.4}$$

Figure 2.2 shows the implications of such a measurement, when combined with the current limits from KamLAND-Zen and EXO. As it can be seen, the current sensitivity is not enough to explore significantly the inverse hierarchy, while Planck data excludes most of the so-called degenerate hierarchy. It follows that the next generation of $\beta\beta0\nu$ experiments must aim for extraordinary sensitivities to the effective neutrino mass. In particular, we will shown that a sensitivity of 20 meV in $m_{\beta\beta}$ is within the reach of a ton-scale HPXe detector. However, with luck, a discovery could make before, if $m_{\beta\beta}$ is near 100 meV.

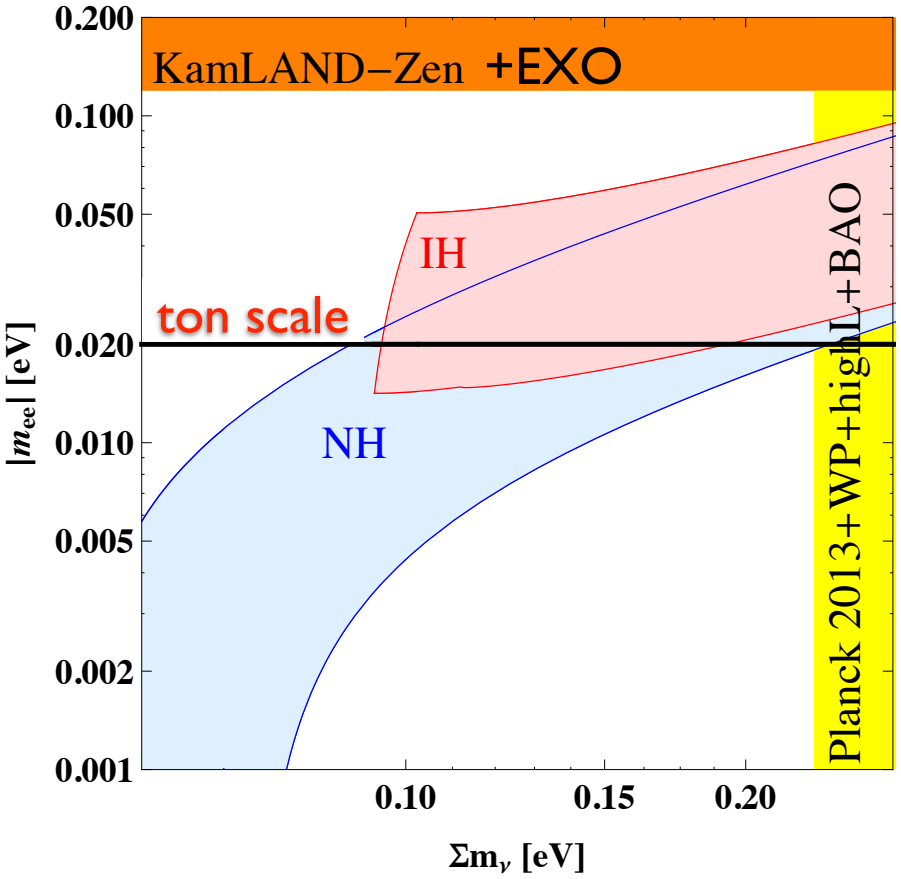

Figure 2.2: The cosmological constraint on the sum of the neutrino mass derived from Planck data, together with the best limits from $\beta\beta0\nu$ experiments (KamLAND-Zen + EXO) and the limit that can be reached by the best experiments in the ton scale, in particular NEXT. Adapted from [22].

In order to gain a feeling of the potential of the NEXT technology is interesting to compare the experimental parameters of the three xenon experiments, which are collected in Table 2.1. The parameters of EXO-200 and KamLAND-Zen are those published by the collaborations [18, 20]. The resolution in NEXT corresponds to the most conservative result obtained by our prototypes [24], and the predicted background rate and efficiency comes from the full background model of the collaboration [14, 25], assuming a conservative background level for the dominant source of background (the energy–plane PMTs). Notice that the background rate of all the experiments is very good. The HPXe technology offers less efficiency than the other two but a much better resolution.

Figure 2.3, shows the expected performance of the three experiments, assuming the

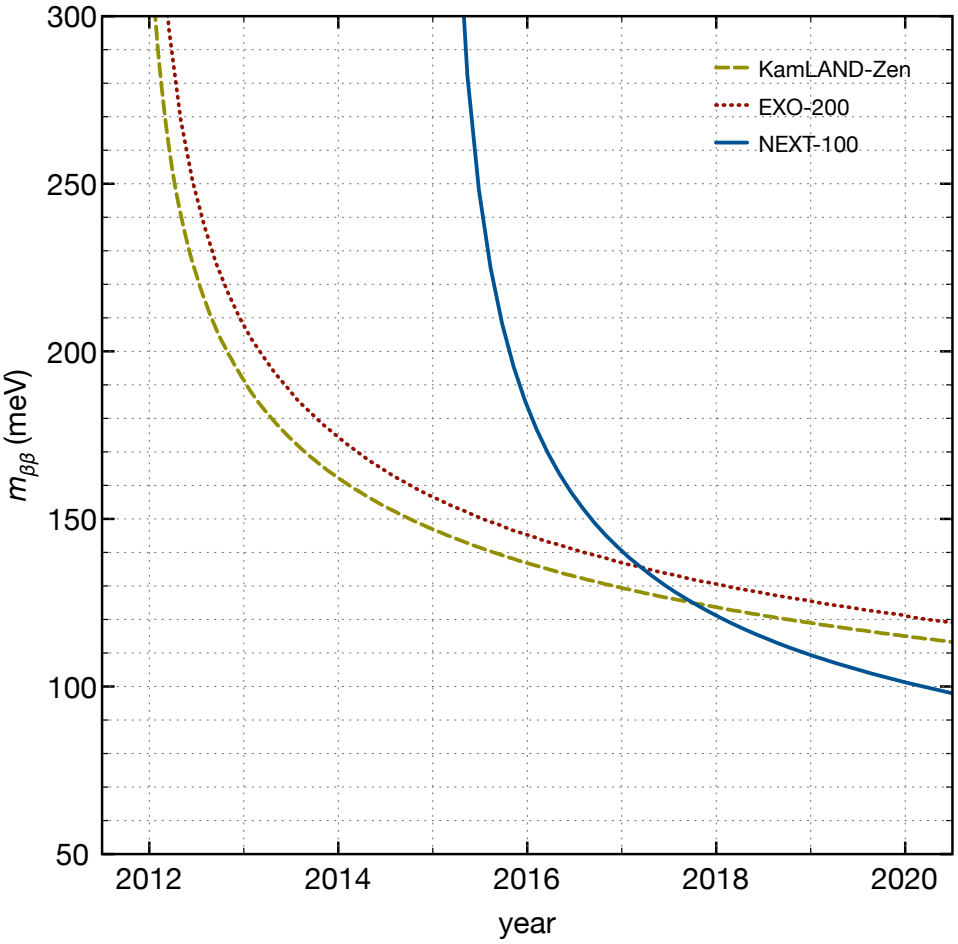

Figure 2.3: Sensitivity of the three xenon experiments as a function of the running time, assuming the parameters described in Table 2.1. We consider a run of 8 years for EXO-200 and KamLAND-Zen (2012 to 2020) and a run of 5 years for NEXT (2015 to 2020).

Table 2.1: Experimental parameters of the three xenon-based double beta decay experiments: (a) total mass of ^{136}Xe, M; (b) enrichment fraction f; (c) signal detection efficiency, ε; (d) energy resolution, δE, at the Q value of ^{136}Xe; and background rate, b, in the region of interest around $Q_{\beta\beta}$ expressed in counts/(keV $\cdot$ kg $\cdot$ y) (shortened as ckky).

Experiment	M (kg)	f (%)	ε (%)	δE (% FWHM)	b (10^{-3} ckky)
EXO-200	110	0.81	0.56	4.0	1.5
KamLAND-Zen	330	0.91	0.42	9.9	1.0
NEXT-100	100	0.91	0.30	0.7	0.5

Table 2.2: Expected experimental parameters of the three xenon-based double beta decay technologies: (a) signal detection efficiency, ε; (b) energy resolution, δE, at the Q value of ^{136}Xe; and background rate, b, in the region of interest around $Q_{\beta\beta}$ expressed in counts/(keV $\cdot$ kg $\cdot$ y).

Experiment	ε (%)	δE (% FWHM)	b (10^{-3} ckky)
LXe	0.38	3.2	0.1
XeSci	0.42	6.5	0.1
HPXe	0.30	0.5	0.1

parameters described in Table 2.1 and the central value of the nuclear matrix elements described in [4]. We consider a run of five years for NEXT (2015 to 2020) and a longer run of eight years for EXO-200 and KamLAND-Zen (2012 to 2020). A total dead-time of 10% a year for all experiments is assumed. It follows that all the three experiment will have a chance of making a discovery if $m_{\beta\beta}$ is in the range of 100 meV. The fact that the experiments are based in different experimental techniques, with different systematic errors, makes their simultaneous running even more attractive. The combination of the three can reach a sensitivity of about 65 meV. Notice that, in spite of its late start, NEXT sensitivity can surpass that of the other xenon experiments.

2.6 Towards the ton scale

To cover the full range allowed by the inverse hierarchy, one needs masses in the range of one ton of isotope, while at the same time detector performance must be improved to extraordinary levels. Xenon experiments have the potential to deploy those large masses (at a cost 10 to 100 times smaller than that needed to obtain other isotopes). This characteristic, together with the fact that one can build large xenon-based TPCs or calorimeters, make them a preferred choice for the next-to-next generation of experiments.

Table 2.2 summarises a projection [26] of the experimental parameters for the three

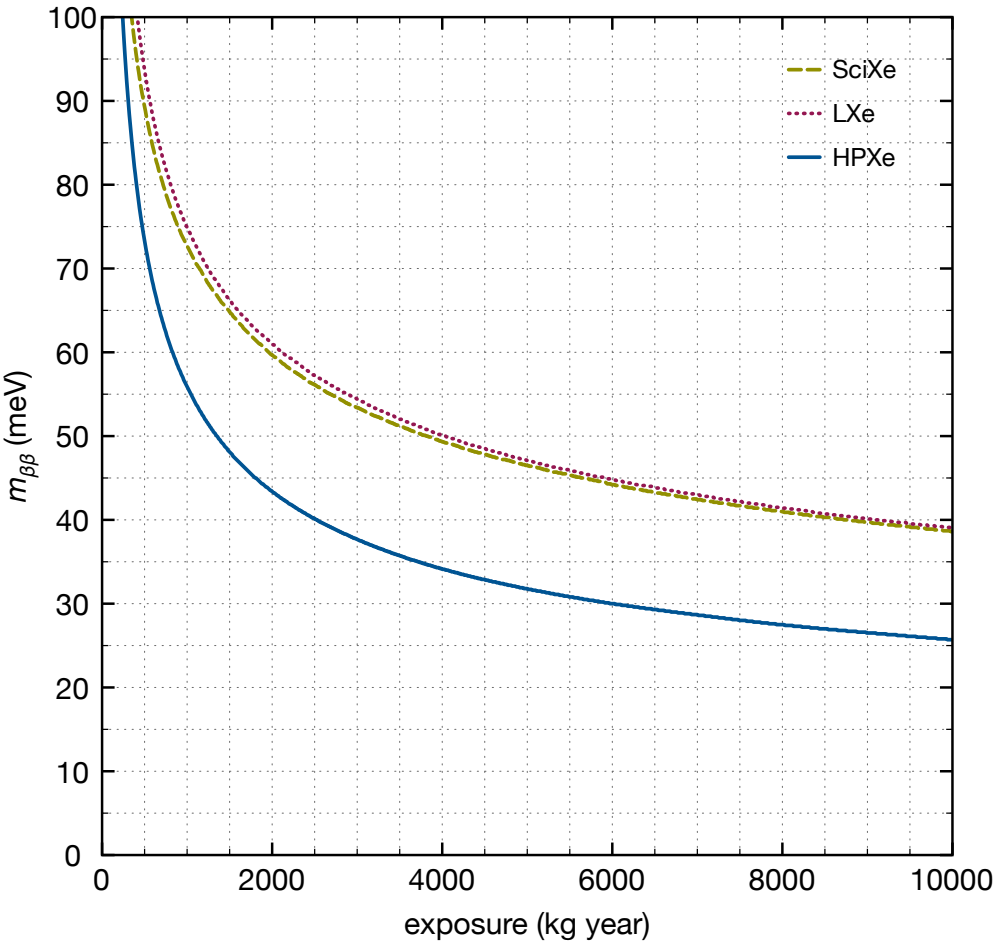

Figure 2.4: Sensitivity of the three technologies experiments as a function of the total exposure, assuming the parameters described in Table 2.2.

technologies, while Figure 2.4, shows the expected performance of xenon experiments assuming the parameters described in Table 2.2, up to a total exposure of 10 ton·year. At the maximum exposure, the LXe and XeSci detectors reach a draw at 40 meV, while the HPXe detector reaches 25 meV.

To summarise, the NEXT experiment has an enormous interest for $\beta\beta0\nu$ searches not only due to its large physics potential — that is the ability to discover that neutrinos are Majorana particles — but also as a springboard to the next-to-next generation of very challenging, ton-based experiments.

Chapter 3

The NEXT-100 detector

3.1 The SOFT concept

As discussed in Chapter 2, next-generation double beta decay experiments have to be sensitive to effective Majorana neutrino masses smaller than 100 meV, and next-to-next generation must reach 20–25 meV if a discovery is not made previously. Designing a detector capable of identifying efficiently and unambiguously such a rare signal is a major experimental challenge.

The NEXT experiment combines excellent energy resolution, a low background rate and the possibility to scale-up the detector to large masses of $\beta\beta$ isotope by using a high-pressure xenon gas (HPXe) electroluminescent time projection chamber (TPC) to search for $\beta\beta0\nu$ in ^{136}Xe. The combination results in excellent sensitivity to $m_{\beta\beta}$.

A major bonus of the NEXT technology is the topological signature. Neutrinoless double beta decay events leave a distinctive topological signature in gaseous xenon: an ionization track, about 30 cm long at 10 bar, tortuous due to multiple scattering, and with larger energy depositions at both ends (see Figure 3.1). The Gotthard experiment [27], consisting in a small xenon gas TPC (5.3 kg enriched to 68% in ^{136}Xe) operated at 5 bar, proved the effectiveness of such a signature to discriminate signal from background.

To achieve optimal energy resolution, the ionization signal is amplified in NEXT using the electroluminescence (EL) of xenon. Also, following ideas introduced in [28] and further developed in our CDR [29], the chamber will have separated detection systems for tracking and calorimetry. This is the so-called *SOFT* concept, illustrated in Figure 3.2. The detection process is as follows: Particles interacting in the HPXe transfer their energy to the medium through ionization and excitation. The excitation energy is manifested in the prompt emission of VUV ($\sim$ 178 nm) scintillation light. The ionization tracks (positive ions and free electrons) left behind by the particle are prevented from recombination by an electric field (0.3–0.5 kV/cm). The ionization electrons drift toward the TPC anode, entering a region, defined by two highly-transparent meshes, with an even more intense electric field (3 kV/cm/bar). There, further VUV photons are generated isotropically by electroluminescence. Therefore, both scintillation and ionization produce an optical signal, to be detected with a sparse plane of PMTs (the

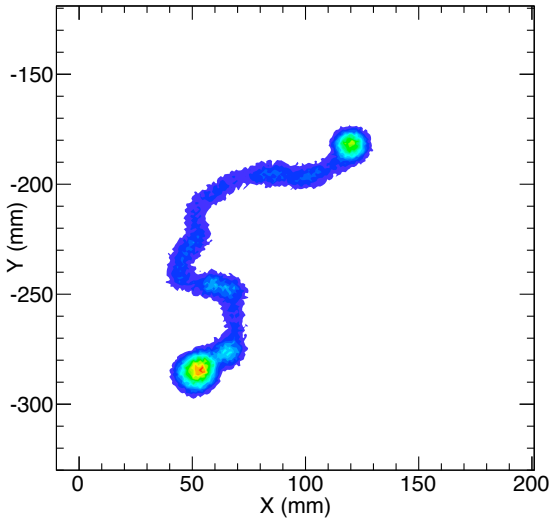

Figure 3.1: Monte-Carlo simulation of a ^{136}Xe $\beta\beta0\nu$ event in xenon gas at 10 bar: the ionization track, about 30 cm long, is tortuous because of multiple scattering, and has larger depositions or *blobs* in both ends.

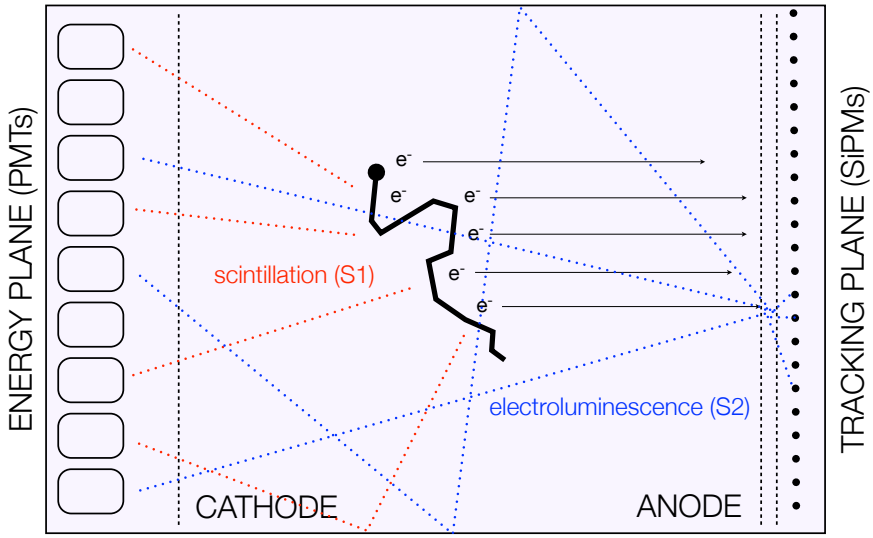

Figure 3.2: The *Separate, Optimized Functions* (SOFT) concept in the NEXT experiment: EL light generated at the anode is recorded in the photosensor plane right behind it and used for tracking; it is also recorded in the photosensor plane behind the transparent cathode and used for a precise energy measurement.

energy plane) located behind the cathode. The detection of the primary scintillation light constitutes the start-of-event, whereas the detection of EL light provides an energy measurement. Electroluminescent light provides tracking as well, since it is detected also a few millimeters away from production at the anode plane, via an array of 1-mm^2 MPPCs, 1-cm spaced (the *tracking plane*).

3.2 The apparatus

Figure 3.3 shows a drawing of the NEXT-100 detector, indicating all the major subsystems. These are:

- The pressure vessel, built in stainless steel and designed to withstand a pressure of 15 bar, described in Subsection 3.2.1. A copper layer on the inside shields the sensitive volume from the radiation originated in the vessel material.
- The field cage, electrode grids, HV penetrators and light tube, described in Subsection 3.2.2.
- The energy plane made of PMTs housed in copper enclosures, described in Subsection 3.2.3.
- The tracking plane made of MPPCs arranged into dice boards (DB), described in Subsection 3.2.4.
- The front end electronics, placed outside the chamber, described in Subsection 3.2.6.
- The gas system, capable of pressurizing, circulating and purifying the gas, described in Subsection 3.2.5.
- Shielding and other infrastructures, described in Subsection 3.2.7.

The NEXT TDR [14] gives the details of the design and components of the detector, which we summarise briefly here.

3.2.1 The pressure vessel

The pressure vessel (PV) consists of a barrel central section with two identical torispheric heads on each end, their main flanges bolted together. The construction material is stainless steel, specifically the low-activity 316Ti alloy. After screening samples, we have secured batches of material in excess of one ton to build the PV. Measurements of 316Ti show very low level of activity (0.2 mBq/kg for the thorium series and 1.3 mBq/kg for the uranium series) [30]. The mass of the PV is 1 200 kg, resulting in a total activity of about 1.6 Bq for the uranium series. To shield this activity we introduce an *inner copper shield* (ICS) 12 cm thick and made of radiopure copper, with an activity of about 5–10 μBq/kg. The ICS will attenuate the radiation coming from the external detector

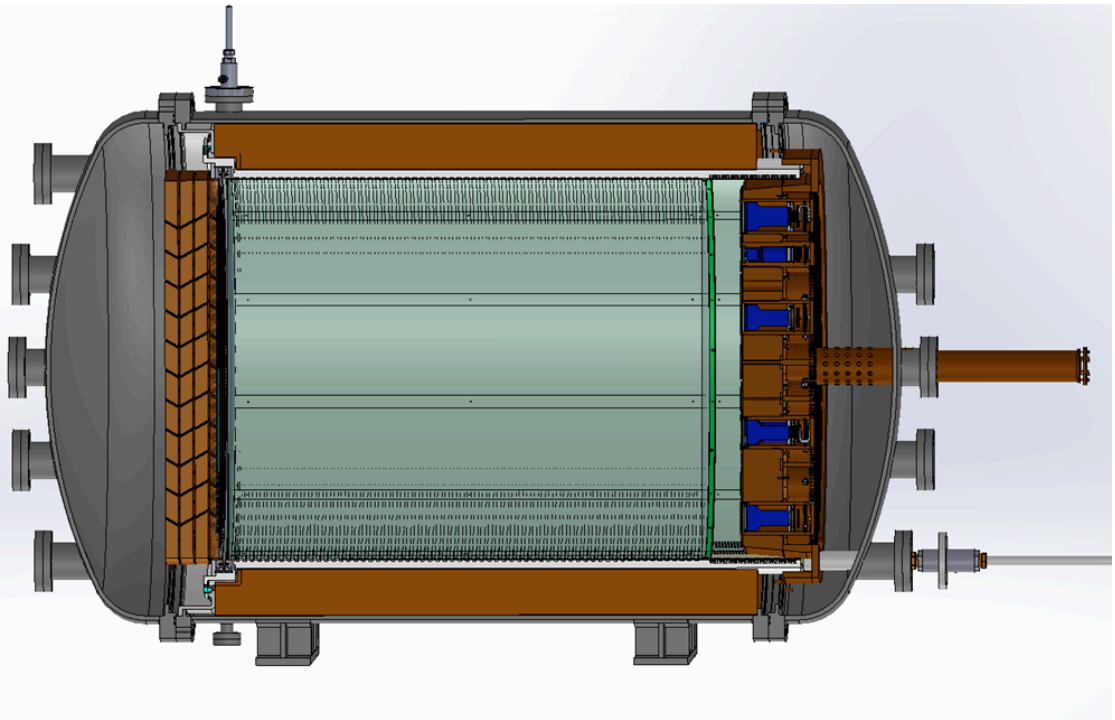

Figure 3.3: A 3D drawing of the NEXT100 detector, showing the pressure vessel (gray), the internal copper shield (brown) and the field cage (green). The PMTs of the energy plane are shown in blue.

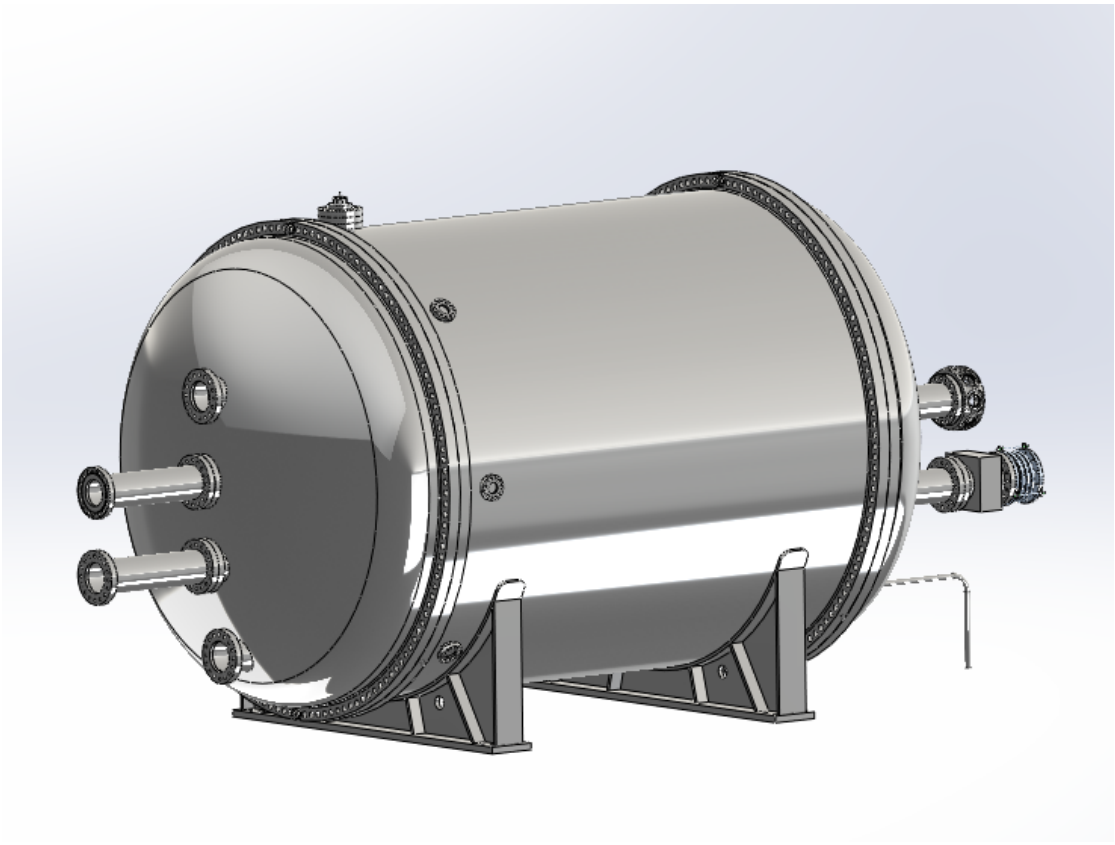

Figure 3.4: A 3D drawing of the pressure vessel.

(including the PV and the external lead shield) by a factor of 100. After the ICS the residual activity due to the PV is about 0.02 Bq. One needs to add the residual activity of the ICS itself which is, taking into account self-shielding, of the order of 0.03 Bq. Thus, the resulting activity of the whole system is ~ 0.05 Bq.

The vessel will be built strictly to *ASME Pressure Vessel Design Code, Section VIII*. It has been designed almost entirely by the collaboration, under the leadership of LBNL and IFIC. The tender for fabrication has adjudicated to the Madrid-based company MOVESA and the preliminaries of fabrication have already started. IFIC is in charge of supervision of fabrication, testing, certification and transport to LSC.

3.2.2 The field cage

The main body of the field cage (Figure 3.5) will be a high-density polyethylene (HDPE) cylindrical shell, 2.5 cm thick, that will provide electric insulation from the vessel. Three wire meshes — cathode, gate and anode — separate the two electric field regions of the detector. The drift region, between cathode and gate, is a cylinder of 107 cm diameter and 130 cm length. Copper strips attached to the HDPE and connected with low background

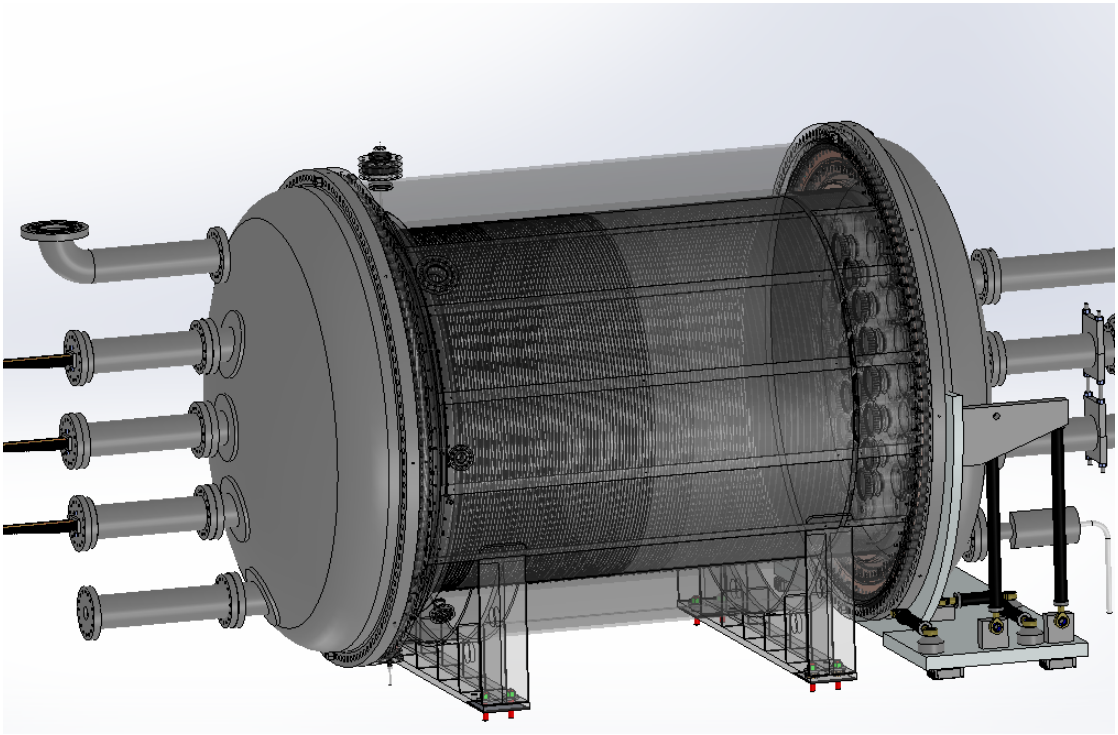

Figure 3.5: A 3D drawing of the detector showing the field cage inside.

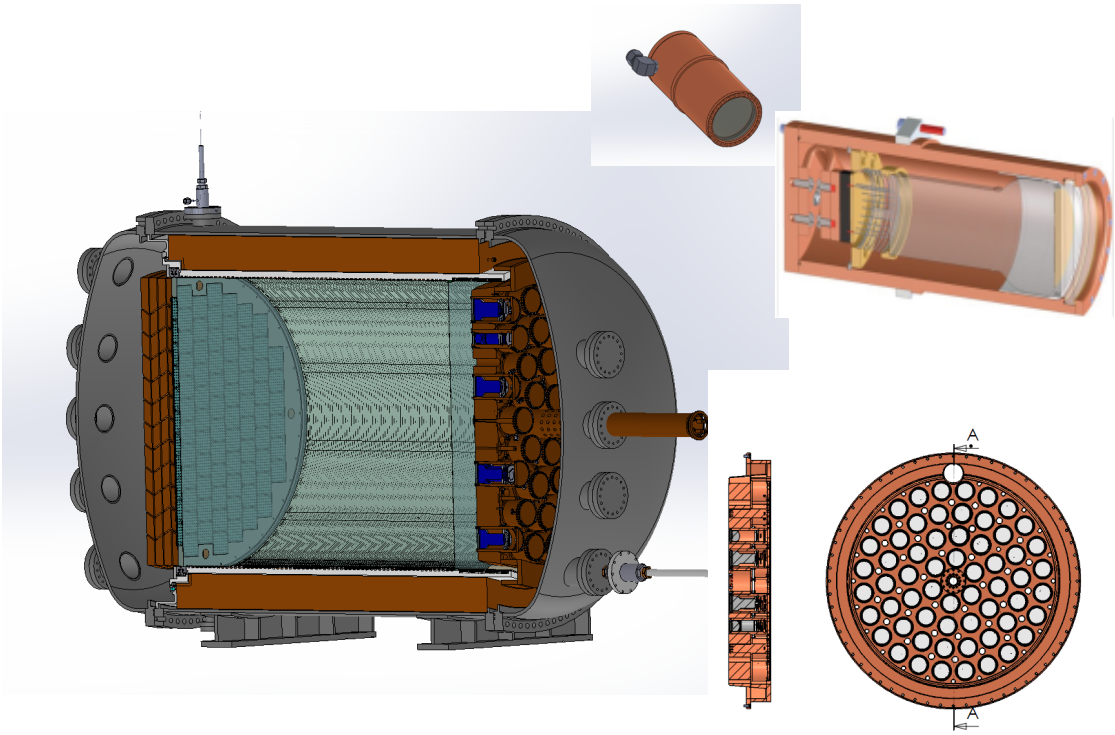

Figure 3.6: A drawing of the detector showing the energy plane inside the PV.

resistors grade the high voltage. The EL region, between gate and anode, is 1.0 cm long.

All the components of the field cage have been prototyped with the NEXT-DEMO detector (see Chapter 4). The NEXT-100 field cage and ancillary systems will be built by our USA collaborators.

3.2.3 The energy plane

The energy measurement in NEXT is provided by the detection of the electroluminescence light by an array of photomultipliers, the *energy plane*, located behind the transparent cathode (Figure 3.6). Those PMTs will also record the scintillation light that indicates the start of the event.

A total of 60 Hamamatsu R11410-10 photomultipliers (Figure 3.7) covering 32.5% of the cathode area constitute the energy plane. This phototube model has been specially developed for radiopure, xenon-based detectors. The manufacturer quoted radioactivity per PMT is 3.3 mBq for the uranium series and 2.3 mBq the thorium series, although independent measurements show even lower activities. The quantum efficiency of the R11410-10 model is around 35% in the VUV and 30% in the blue region of the spectrum, and the dark count rate is 2–3 kHz (0.3 photoelectron threshold) at room temperature [31].

Pressure-resistance tests run by the manufacturer showed that the R11410-10 cannot withstand pressures above 6 atmospheres. Therefore, in NEXT-100 they will be sealed

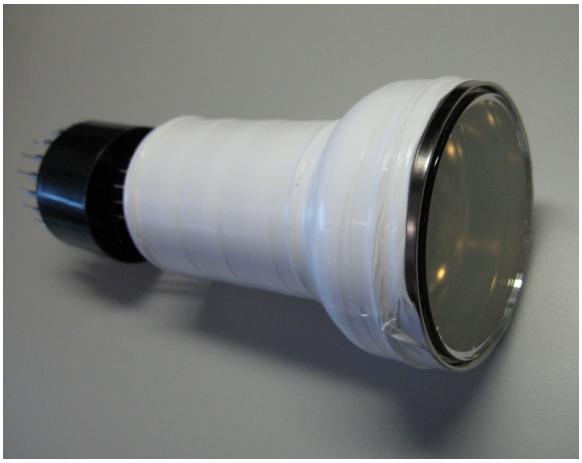

Figure 3.7: The Hamamatsu R11410-10, a 3-inches photomultiplier with high quantum efficiency ($> 30\%$) at the xenon scintillation wavelengths and low radioactivity.

into individual pressure resistant, vacuum tight copper enclosures coupled to sapphire windows (see Figure 3.8). The window, 5 mm thick, is secured with a screw-down ring and sealed with an O-ring to the front-end of the enclosure. A similar back-cap of copper seals the back side of the enclosures. The PMT is optically coupled to the window using silicone optical pads of 2–3 mm thickness. A spring on the backside pushes the photomultiplier against the optical pads.

These PMT modules are all mounted to a common carrier plate that attaches to an internal flange of the pressure vessel head (see Figure 3.9). The enclosures are all connected via individual pressure-resistant, vacuum-tight tubing conduits to a central manifold, and maintained at vacuum well below the Paschen minimum, avoiding sparks and glow discharge across PMT pins. The PMT cables route through the conduits and the central manifold to a feedthrough in the pressure vessel nozzle.

The design of the energy plane has been shared between IFIC, UPV (Universidad Politécnica de Valencia) and LBNL groups. The PMTs have already been purchased and tested, and are currently being screened for radioactivity at the LSC. Prototype PMT enclosures have been built and a full prototype energy plane including 14 PMTs is under construction and will be tested at the LSC in 2013. If sufficient funds are available the full energy plane will be installed in the detector during 2014.

3.2.4 The tracking plane

The tracking function in NEXT-100 will be provided by a plane of multi-pixel photon counters (MPPCs) operating as sensor pixels and located behind the transparent EL gap. The chosen MPPC is the S10362-11-050P model by Hamamatsu. This device has an active area of 1 mm^2, 400 sensitive cells (50 μm size) and high photon detection efficiency in the blue region (about $\sim 50\%$ at 440 nm). MPPCs are very cost-effective and their radioactivity is very low, given its composition (mostly silicon) and very small mass.

Figure 3.8: The pressure-resistant enclosure, or "can" protecting the PMTs inside the PV.

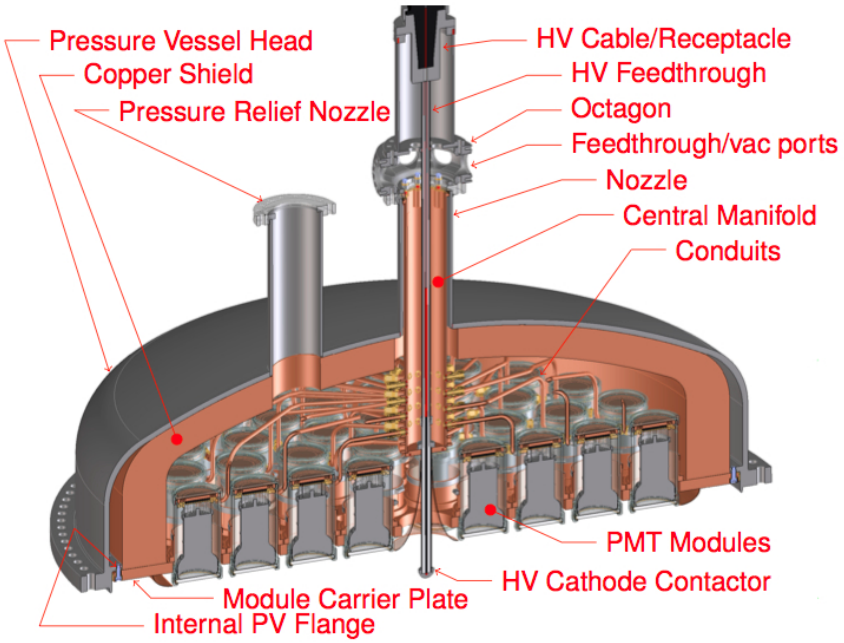

Figure 3.9: The full energy plane of NEXT-100 mounted in the vessel head.

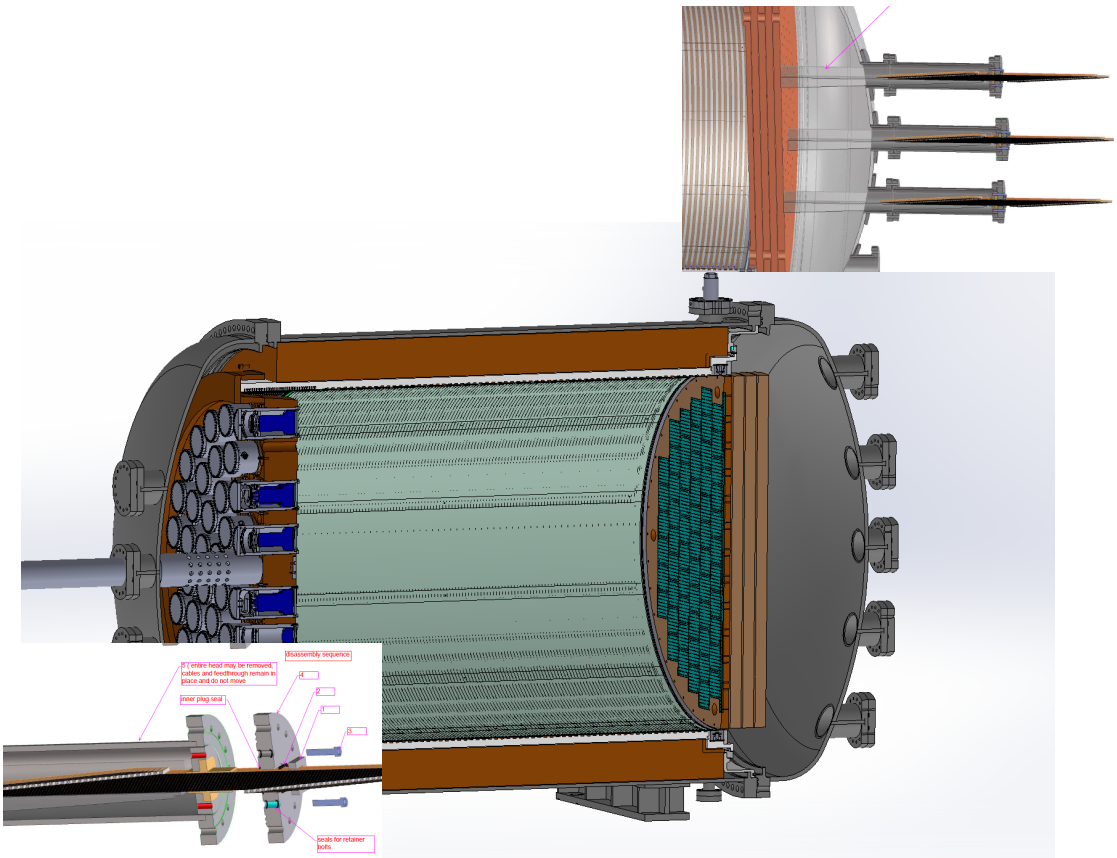

Figure 3.10: A 3D drawing of the detector showing the tracking plane inside, including the feedthroughs to extract the cables carrying the signals from the MPPCs.

The MPPCs will be mounted in Dice Boards (DB), identical to those prototyped in NEXT-DEMO (see Chapter 4). The electronics for the MPPCs will also be an improved version of the electronics for the DEMO detector. Also, like in NEXT-DEMO, all the electronics will be outside the chamber. The large number of channels in NEXT-100, on the other hand, requires the design and fabrication of large custom-made feedthroughs (LCFT) to extract the signals, as illustrated in Figure 3.10.

The ∼8 000 MPPCs needed for the tracking plane have already been purchased. The design of the DBs and the FEE have been made at the IFIC and UPV. The DBs have been fully tested in NEXT-DEMO and are ready for production.

A prototype of the LCFT will be tested in 2013. The full tracking plane can be installed in 2014.

3.2.5 The gas system

The gas system must be capable of pressurizing, circulating, purifying, and depressurizing the NEXT-100 detector with xenon, argon and possibly other gases with negligible loss and without damage to the detector. In particular, the probability of any substantial loss of the very expensive enriched xenon (EXe) must be minimized. A list of requirements, in approximate decreasing order of importance, considered during the design is given below:

1. Pressurize vessel, from vacuum to 15 bar (absolute).
2. Depressurize vessel to closed reclamation system, 15 bar to 1 bar (absolute), on fault, in 10 seconds maximum.
3. Depressurize vessel to closed reclamation system, 15 bar to 1 bar (absolute), in normal operation, in 1 hour maximum.
4. Relieve pressure (vent to closed reclamation system) for fire or other emergency condition.
5. Allow a maximum leakage of EXe through seals (total combined) of 100 g/year.
6. Allow a maximum loss of EXe to atmosphere of 10 g/year.
7. Accommodate a range of gasses, including Ar and N_2.
8. Circulate all gasses through the detector at a maximum rate of 200 standard liters per minute (slpm) in axial flow pattern.
9. Purify EXe continuously. Purity requirements: < 1 ppb O_2, CO_2, N_2, CH_4.

The most vulnerable component of the gas system is the re-circulation compressor, that must have sufficient redundancy to minimize the probability of failure and leakage. The collaboration has chosen a compressor manufactured by SERA COMPRESS GMBH. This compressor is made with metal-to-metal seals on all the wetted surfaces. The gas is

moved through the system by a triple stainless steel diaphragm. Between each of the diaphragms there is a sniffer port to monitor for gas leakages. In the event of a leakage, automatic emergency shutdown can be initiated.

MicroTorr model MC4500-902FV from SAES has been chosen as the purification filter for PS4-MT15 from SAES will be needed (since they result in a longer electron lifetime and do not emit radon) for the enriched xenon run.

An automatic recovery system of the expensive EXe will also be needed to evacuate the chamber in case of an emergency condition. A 30-m^3 expansion tank will be placed inside the laboratory to quickly reduce the gas pressure in the system. Additionally, we will implement a similar solution to that proposed by the LUX collaboration, where a chamber permanently cooled by liquid nitrogen will be used.

The gas system has been designed as a collaboration between IFIC and University of Zaragoza (UNIZAR), taking advantage of the experience gained with our prototypes. The basic gas system needed for the initial operation of the NEXT-100 apparatus has already been purchased and shipped to the LSC, but the system must be upgraded during 2014 for the enriched xenon run in 2015.

3.2.6 Electronics

The NEXT-100 data-acquisition system (DAQ) follows a modular architecture named the Scalable Readout System (SRS), already described in our CDR [29]. At the top of the hierarchy, a PC farm running the DAQ software, DATE, receives event data from the DAQ modules via Gigabit Ethernet (GbE) links. The DATE PCs (Local Data Concentrators, LDCs) assemble incoming fragments into sub-events, which are sent to one or more additional PCs (Global Data Concentrators, GDC). The GDCs build complete events and store them to disk for offline analysis.

The DAQ modules used are Front-End Concentrator (FEC) cards, which serve as the generic interface between the DAQ system and application-specific front-end modules. The FEC module can interface different kinds of front-end electronics by using the appropriate plug-in card. The FEC card and the overall SRS concept have been developed within the framework of the CERN RD-51 collaboration. Three different FEC plug-in cards are used in NEXT-100.

Electronics for the energy plane

The front-end (FE) electronics for the PMTs in NEXT-100 will be very similar to the system developed for the NEXT-DEMO and NEXT-DBDM prototypes. The first step in the chain is to shape and filter the fast signals produced by the PMTs (less than 5 ns wide) to match the digitizer and eliminate the high frequency noise. An integrator is implemented by simply adding a capacitor and a resistor to the PMT base. The charge integration capacitor shunting the anode stretches the pulse and reduces the primary signal peak voltage accordingly.

Our design uses a single amplification stage based on the fully differential amplifier THS4511, which features low noise (2 nV/$\sqrt{\text{Hz}}$) and provides enough gain to compensate

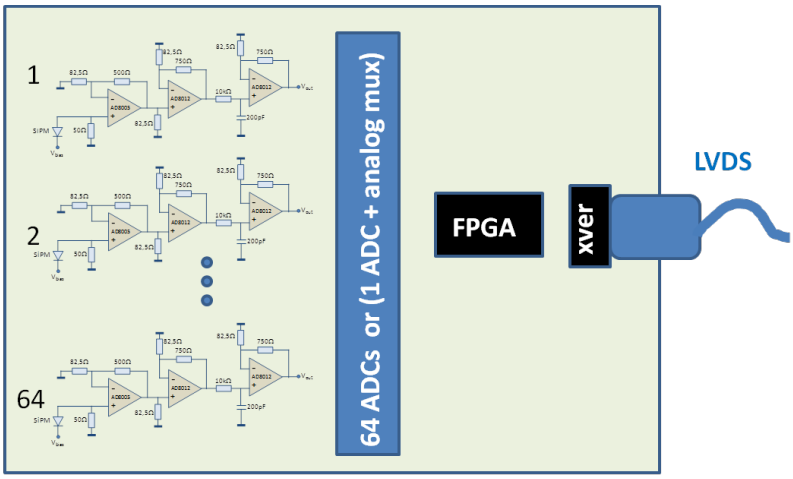

Figure 3.11: Functional blocks in the FEB card.

for the attenuation in the following stage, based on a passive RC filter with a cut frequency of 800 kHz. This filtering produces enough signal stretching to allow acquiring many samples per single photo-electron at 40 MHz.

Electronics for the tracking plane

The tracking plane will have $\sim$ 8 000 channels. On the other hand, the electronics for the MPPCs is simplified given the large gain of these devices. Our design consists of a very simple, 64 channel Front-End Board (FEB, Figure 3.11). Each FEB takes the input of a single DB (transmitted via low-crosstalk kapton flat cables) and includes the analog stages, ADC converters, voltage regulators and an FPGA that handles, formats, buffers and transmits data to the DAQ. LVDS clock and trigger inputs are also needed. A total of 110 FEBs are required. The architecture of the FEB is described in our TDR.

The design of the electronics is a collaboration between UPV and LBNL. It will be an evolution of the electronics currently operational at NEXT-DEMO. The DAQ is responsibility of UPV, and it will also be an improved version of the DEMO DAQ.

3.2.7 Shielding and other infrastructures

To shield NEXT-100 from the external flux of high-energy gamma rays a relatively simple lead castle, shown in Figure 3.12, has been chosen, mostly due to its simplicity and cost-effectiveness. The lead wall has a thickness of 20 cm and is made of layers of staggered lead bricks held with a steel structure. The lead bricks have standard dimensions ($200 \times 100 \times 50$ mm^3), and, by requirement, an activity in uranium and thorium lower than 0.4 mBq/kg.

The lead castle is made of two halves mounted on a system of wheels that move on rails with the help of an electric engine. The movable castle has an open and a closed position. The former is used for the installation and service of the pressure vessel; the

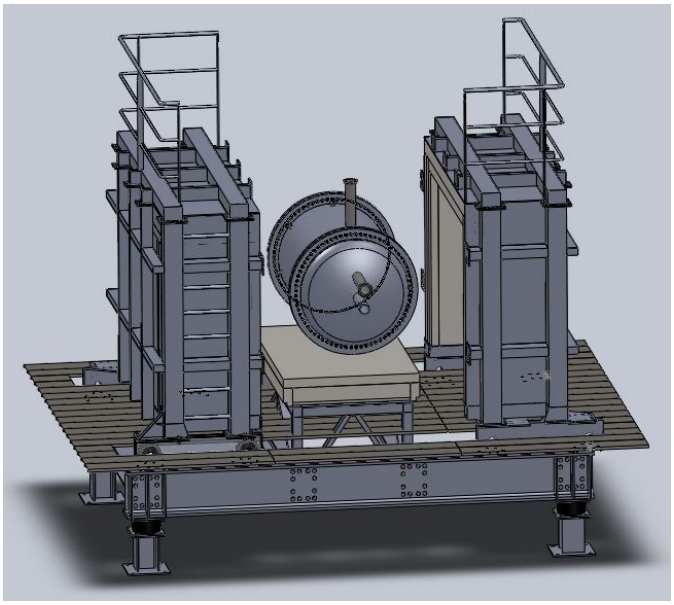

Figure 3.12: Drawing of the NEXT-100 lead castle shield in its open configuration.

latter position is used in normal operation. A lock system fixes the castle to the floor in any of the two configurations to avoid accidental displacements.

The design of the lead castle has been led by the University of Girona (UdG), in collaboration with UPV and IFIC. The design is completed and the shield is ready to be built pending the availability of funds.

The construction of the infrastructures needed for the NEXT-100 experiment (working platform, seismic pedestal) is currently underway. They will be fully installed at the LSC by the end of 2013.

Figure 3.13 shows an image of Hall A, future location of NEXT-100. The pool-like structure is intended to be a catchment reservoir to hold xenon or argon — a liquid-argon experiment, ArDM, will be neighbouring NEXT-100 in Hall A — gas in the event of a catastrophic leak. Therefore, for reasons of safety all experiments must preclude any personnel working below the level of the top of the catchment reservoir.

An elevated working platform will be built prior to the installation of NEXT-100. It is designed to stand a uniform load of 1500 kg/m^2 and a concentrated load of 200 kg/m^2. It is anchored to the hall ground and walls. The platform floor tiles are made of galvanized steel and have standard dimension to minimize cost.

Due to the mild seismic activity of the part of the Pyrenees where the LSC is located, a comprehensive seismic study has been conducted as part of the project risk analysis. As a result, an anti-seismic structure that will hold both pressure vessel and shielding has been designed. This structure will be anchored directly to the ground and independent of the working platform to allow seismic displacements in the event of an earthquake.

Figure 3.14 shows the placement of NEXT-100 and components on the platform as

Figure 3.13: View of Hall A of the Laboratorio Subterráneo de Canfranc prior to any equipment installation.

well as the dimensions.

3.3 NEXT background model

Every $\beta\beta0\nu$ experiment must have a model that describes the sources of radioactive contaminants and their activity, as well as a detailed simulation that allows to predict the fraction of background events that are misidentified as signal. The ensemble of data and calculations is called the experiment background model.

3.3.1 Sources of background

Radioactive contaminants in detector materials

After the decay of ^{214}Bi, the daughter isotope, ^{214}Po, emits a number of de-excitation gammas with energies above 2.3 MeV. The gamma line at 2447 keV, of intensity 1.57%, is very close to the Q-value of ^{136}Xe. The gamma lines above $Q_{\beta\beta}$ have low intensity and their contribution is negligible.

The daughter of ^{208}Tl, ^{208}Pb, emits a de-excitation photon of 2614 keV with a 100% intensity. The Compton edge of this gamma is at 2382 keV, well below $Q_{\beta\beta}$. However, the scattered gamma can interact and produce other electron tracks close enough to the initial Compton electron so they are reconstructed as a single object falling in the energy region of interest (ROI). Photoelectric electrons are produced above the ROI but can loose energy via bremsstrahlung and populate the window, in case the emitted photons escape out of the detector. Pair-creation events are not able to produce single-track events in the ROI.

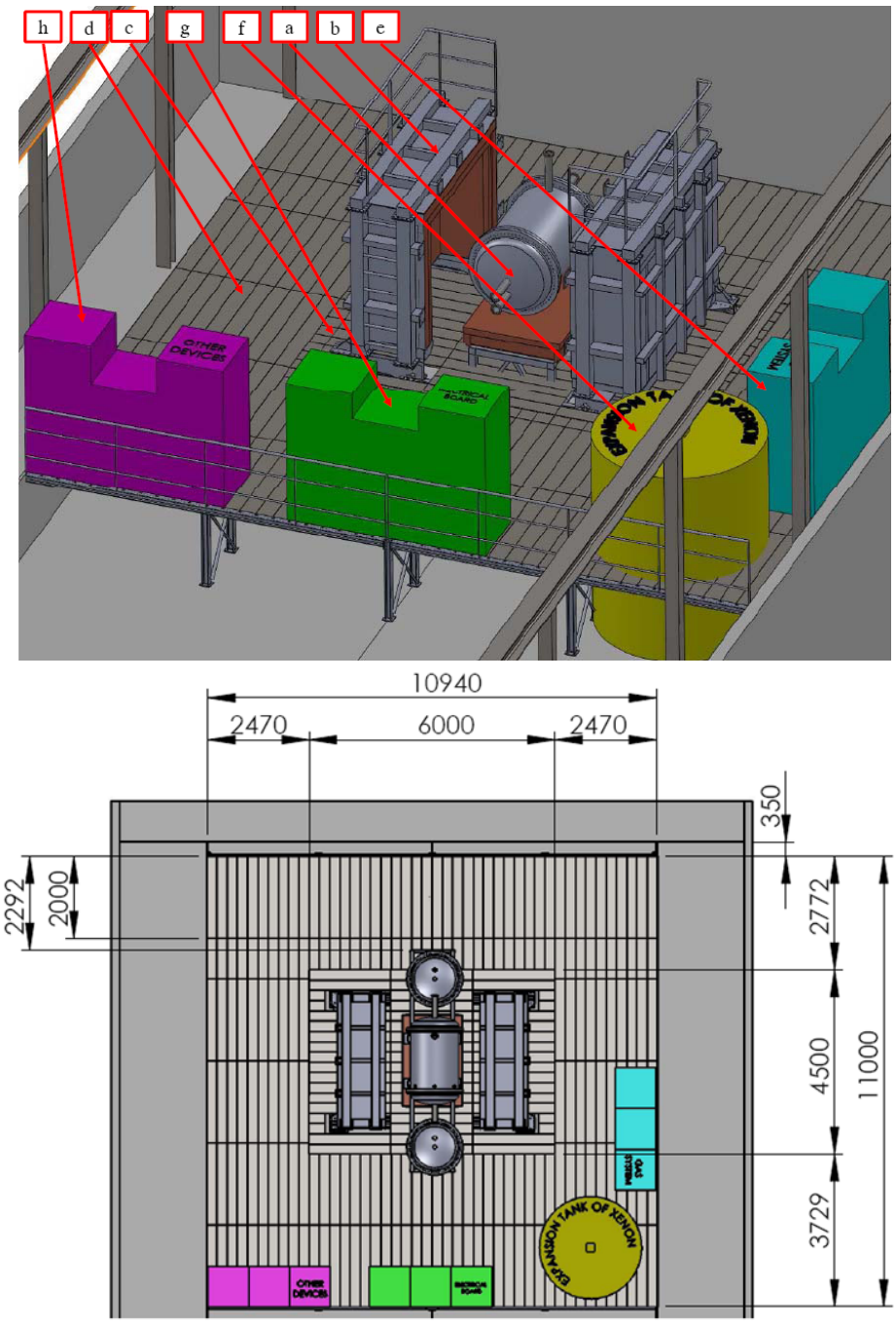

Figure 3.14: Top: Intended location of the components and subsystems for the operation of NEXT-100 on the working platform: (a) NEXT-100; (b) the lead castle shield in its open configuration; (c) seismic platform; (d) working platform; (e) gas purification system; (f) emergency gas vent tank; (g) data acquisition system; (h) other systems. Bottom: Top view showing the dimensions of the working platform.

Radon

Radon constitutes a dangerous source of background due to the radioactive isotopes ^{222}Rn (half-life of 3.8 d) from the ^{238}U chain and ^{220}Rn (half-life of 55 s) from the ^{232}Th chain. As a gas, it diffuses into the air and can enter the detector. ^{214}Bi is a decay product of ^{222}Rn, and ^{208}Tl a decay product of ^{220}Rn. In both cases, radon undergoes an alpha decay into polonium, producing a negative ion which is drifted towards the anode by the electric field of the TPC. As a consequence, ^{214}Bi and ^{208}Tl contaminations can be assumed to be deposited on the anode surface. Radon may be eliminated from the TPC gas mixture by recirculation through appropriate filters. There are also ways to suppress radon in the volume defined by the shielding. Radon control is a major task for a $\beta\beta0\nu$ experiment, and will be of uppermost importance for NEXT-100.

Cosmic rays and laboratory rock backgrounds

Cosmic particles can also affect our experiment by producing high energy photons or activating materials. This is the reason why double beta decay experiments are conducted deep underground. At these depths, muons are the only surviving cosmic ray particles, but their interactions with the rock produce neutrons and electromagnetic showers. Furthermore, the rock of the laboratory itself is a rather intense source of ^{208}Tl and ^{214}Bi backgrounds as well as neutrons.

The flux of photons emanating from the LSC walls is (see our TDR and references therein):

- 0.71 ± 0.12 $\gamma/\mathrm{cm}^2/\mathrm{s}$ from the ^{238}U chain.
- 0.85 ± 0.07 $\gamma/\mathrm{cm}^2/\mathrm{s}$ from the ^{232}Th chain.

These measurements include all the emissions in each chain. The flux corresponding to the ^{208}Tl line at 2614.5 keV and the flux corresponding to the ^{214}Bi line at 1764.5 keV were also measured (from the latter it is possible to deduce the flux corresponding to the 2448 keV line). The results are:

- 0.13 ± 0.01 $\gamma/\mathrm{cm}^2/\mathrm{s}$ from the ^{208}Tl line.
- 0.006 ± 0.001 $\gamma/\mathrm{cm}^2/\mathrm{s}$ from the ^{214}Bi line at 2448 keV.

The above backgrounds are considerably reduced by the shielding. In addition, given the topological capabilities of NEXT, the residual muon and neutron background do not appear to be significant for our experiment.

3.3.2 Radioactive budget of NEXT-100

Information on radiopurity of the materials expected to be used in the construction of NEXT100 has been compiled, performing specific measurements and also examining data from the literature for materials not yet screened. A detailed description is presented in [30]. A brief summary of the results presented there is shown in Table 3.1.

Table 3.1: Activity (in mBq/kg) of the most relevant materials used in NEXT.

Material	Subsystem	^{238}U	^{232}Th
Lead Shield	0.37	0.07	
Copper	ICS	< 0.012	< 0.004
Steel (316Ti)	PV	< 1.9	< 1
Inconel 718	PV	< 5.6	< 13.8
Inconel 625	PV	< 2.4	< 6.0
Peek	FC/EP/TP	36	11.7
Capacitors (Tantalum)	FC/EP/TP	320	1.23×10^3
SMD Resistors, Finechem (per pc)	FC	0.022	0.048
Polyethylene	FC	0.23	¡0.14
TTX	LT	12.4	1.6
TPB	LT/EP/TP	1.63	0.47
PTFE (Teflon)	EP/TP/DB	0.025	0.031
PMT (R11410-MOD per pc)	EP	< 2.5	< 2.5
PMT (R11410-MOD per pc)	EP	< 0.4	< 0.3
Sapphire window	EP	0.31	0.12
CUFLON	TP	0.36	0.28
Kapton cable	TP/EP	14	39

3.3.3 Expected background rate

As already remarked, NEXT has two powerful handles to distinguish signal from background:

- *Energy resolution*: Signal events have all the same energy. Selecting only the events in the energy region around $Q_{\beta\beta}$ defined by the resolution eliminates most of the spurious activity in the detector.

- *Event topology*: Signal events appear uniformly distributed in the source (i.e., the enriched xenon) and have a distinctive topology (a twisted track with blobs in both ends, see Figure 3.1). Requiring signal events to be strictly contained in the active volume of the chamber eliminates essentially all charged backgrounds entering the detector. Confined tracks generated by neutral particles, like high-energy, gammas can be suppressed by pattern recognition.

As explained above, the only relevant backgrounds for NEXT are the photons emitted by the ^{208}Tl line (2614.5 keV) and the ^{214}Bi line (2448 keV). These sit very near $Q_{\beta\beta}$ and the interaction of the photons in the gas can fake the $\beta\beta0\nu$ signal. NEXT-100 has the structure of a Matryoshka (a Russian nesting doll). The flux of gammas emanating from the LSC walls is drastically attenuated by the lead castle (LC), and the residual flux, together with that emitted by the lead castle itself and the materials of the pressure

Table 3.2: Acceptance of the selection cuts for signal and backgrounds.

	Fraction of events		
Selection cut	$\beta\beta0\nu$	^{214}Bi	^{208}Tl
Confined, single track	0.48	6.0×10^{-5}	2.4×10^{-3}
Energy ROI	0.33	2.2×10^{-6}	1.9×10^{-6}
Topology $\beta\beta0\nu$	0.25	1.9×10^{-7}	1.8×10^{-7}

vessel is further attenuated by the inner copper shielding (ICS). The ICS also attenuates the flux emitted by the tracking plane FE electronics (FEE), which sit behind it. One then needs to add the contributions of the "inner elements" in NEXT: field cage (FC), energy plane (EP), and the elements of the tracking plane (TP) not shielded by the ICS.

A detailed Geant4 simulation of the NEXT-100 detector was written in order to compute the background rejection factor achievable with the detector. Simulated events, after reconstruction, were accepted as a $\beta\beta0\nu$ candidate if

(a) they were reconstructed as a single track confined within the active volume;

(b) their energy fell in the region of interest, defined as ±0.5 FWHM around $Q_{\beta\beta}$;

(c) the spatial pattern of energy deposition corresponded to that of a $\beta\beta0\nu$ track (*blobs* in both ends).

The achieved background rejection factor together with the selection efficiency for the signal are shown in Table 3.2. As can be seen, the cuts suppress the radioactive background by more than 7 orders of magnitude. This results in an estimated background rate of about 5×10^{-4} counts/(keV $\cdot$ kg $\cdot$ y).

Chapter 4

The NEXT EL prototypes

4.1 NEXT Prototypes

To prove the innovative concepts behind the NEXT design, a number of prototypes have been built. These are:

- *NEXT-DBDM*, operating at LBNL. This was our first operative prototype and has demonstrated a superb resolution, that extrapolates to 0.5% FWHM at $Q_{\beta\beta}$.
- *NEXT-DEMO*, operating at IFIC. This is a larger prototype, which can hold a mass similar to that of the Gotthard experiment. It is conceived to fully test and demonstrate the EL technology. It is described in more detail in the next section.
- *NEXT-MM*, a prototype initially used to test the Micromegas technology and currently used to explore new gas mixtures. NEXT-MM operates at the University of Zaragoza.

The two EL prototypes (NEXT-DBDM and NEXT-DEMO) are fully operational since 2011. The description of these prototypes and the initial results obtained with them have recently been published [24, 32, 33]. The NEXT-MM prototype is currently being commissioned at low pressure.

4.2 NEXT-DEMO

In this section we describe in more detail the NEXT-DEMO demonstrator and our first results. The main goal of the prototype was the demonstration of the detector concept to be used in NEXT-100, more specifically:

1. To demonstrate good energy resolution (better than 1% FWHM at $Q_{\beta\beta}$) in a large system with full spatial corrections.
2. To demonstrate track reconstruction and the performance of MPPCs.

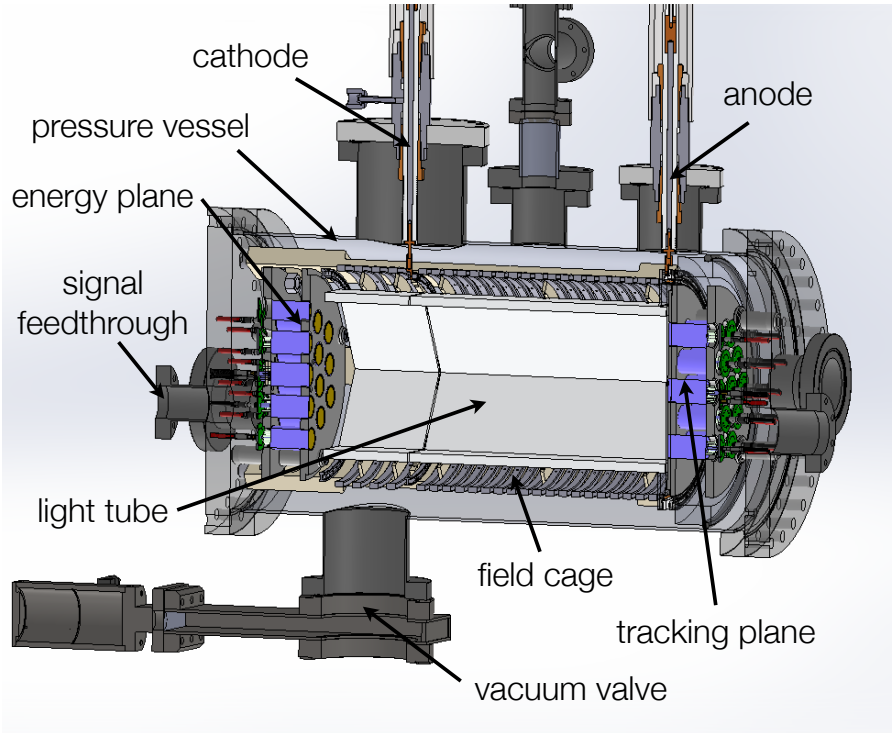

Figure 4.1: Cross-section drawing of the NEXT-DEMO detector with all major parts labelled.

3. To test long drift lengths and high voltages (up to 50 kV in the cathode and 25 kV in the anode).

4. To understand gas recirculation in a large volume, including operation stability and robustness against leaks.

5. To understand the transmittance of the light tube, with and without wavelength shifter.

The apparatus, shown in figure 4.1, is a high-pressure xenon electroluminescent TPC implementing the NEXT concept. Its active volume is 30 cm long. A tube of hexagonal cross section made of PTFE is inserted into the active volume to improve the light collection. The TPC is housed in a stainless-steel pressure vessel, 60 cm long and with a diameter of 30 cm, that can withstand up to 15 bar. Natural xenon circulates in a closed loop through the vessel and a system of purifying filters. The detector is not radiopure and is not shielded against natural radioactivity. It is installed in a semi-clean room (see Figure 4.2) at IFIC, in Valencia, Spain.

The time projection chamber itself is shown in Figure 4.3. Three metallic wire grids — called *cathode*, *gate* and *anode* — define the two active regions: the 30-cm long *drift region*, between cathode and gate; and the 0.5-cm long *EL region*, between gate and

Figure 4.2: The NEXT-DEMO detector and ancillary systems (gas system, front-end electronics and DAQ) in their location in a semi-clean room at IFIC.

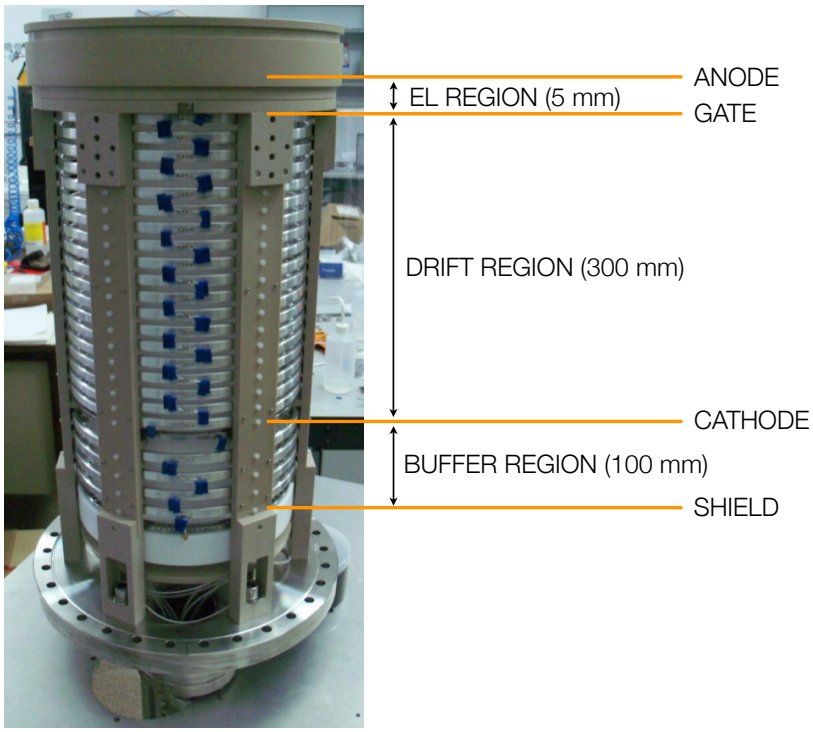

Figure 4.3: External view of the time projection chamber mounted on one end-cap. The approximate positions of the different regions of the TPC are indicated.

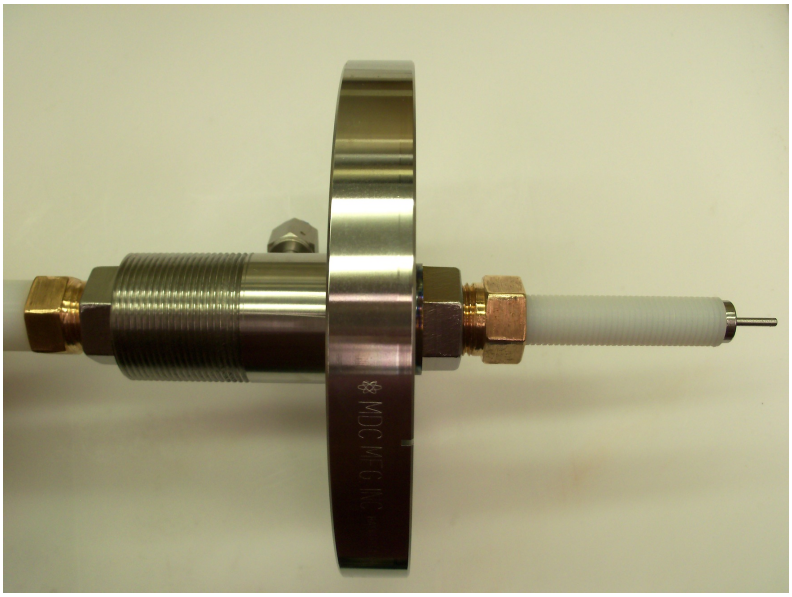

Figure 4.4: The NEXT-DEMO high-voltage feed-through, designed and built by Texas A&M.

anode. The electric field is created by supplying a large negative voltage to the cathode, then degrading it using a series of metallic rings of 30 cm diameter spaced 5 mm and connected via 0.5 GΩ resistors. The gate is at negative voltage so that a moderate electric field — typically of 2.5 to 3 kV cm^{-1} bar^{-1} — is created between the gate and the anode, which is at ground. A *buffer region* of 10 cm between the cathode and the energy plane protects this from the high-voltage by degrading it safely to ground potential.

The high voltage is supplied to the cathode and the gate through custom-made high-voltage feed-throughs (HVFT), shown in Figure 4.4, built pressing a stainless-steel rod into a Tefzel (a plastic with high dielectric strength) tube, which is then clamped using plastic ferrules to a CF flange. They have been tested to high vacuum and 100 kV without leaking or sparking.

A set of six panels made of PTFE (Teflon) are mounted inside the electric-field cage forming a *light tube* of hexagonal cross section (see Figure 4.5) with an apothem length of 8 cm. PTFE is known to be an excellent reflector in a wide range of wavelengths [34], thus improving the light collection efficiency of the detector. In a second stage, the panels were vacuum-evaporated with TPB — which shifts the UV light emitted by xenon to blue ($\sim$ 430 nm) — in order to study the improvement in reflectivity and light detection. Figure 4.5 (right panel) shows the light tube illuminated with a UV lamp after the coating.

Six bars manufactured from PEEK, a low outgassing plastic, hold the electric-field cage and the energy plane together. The whole structure is attached to one of the end-caps using screws, and introduced inside the vessel with the help of a rail system. All the TPC structures and the HVFT were designed and built by Texas A&M.

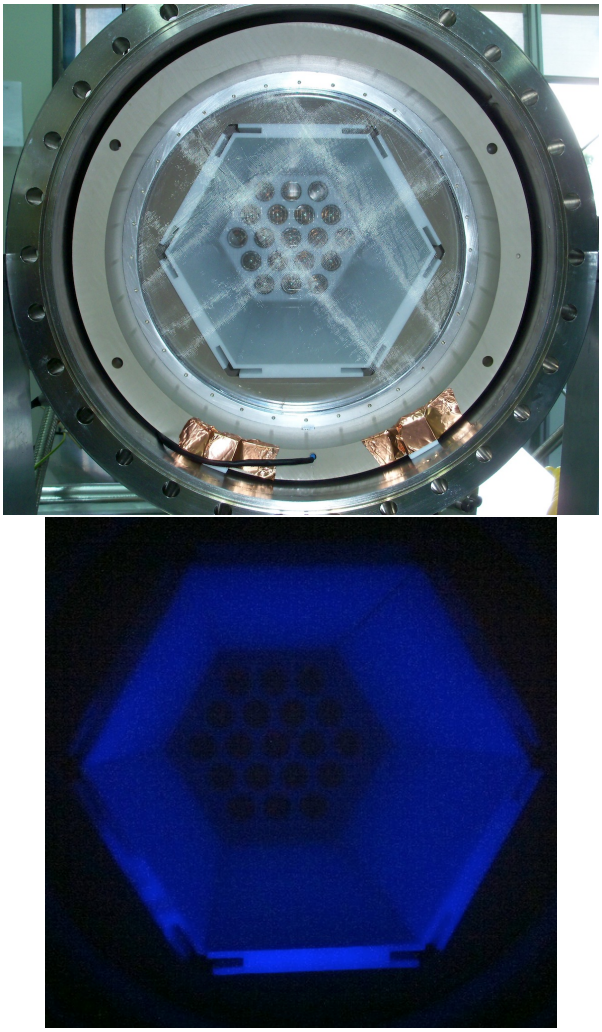

Figure 4.5: View of the light tube from the position of the tracking plane. Left: The meshes of the EL region can be seen in the foreground, and in the background, at the end of the light tube, the PMTs of the energy plane are visible. Right: The light tube of NEXT-DEMO illuminated with a UV lamp after being coated with TPB.

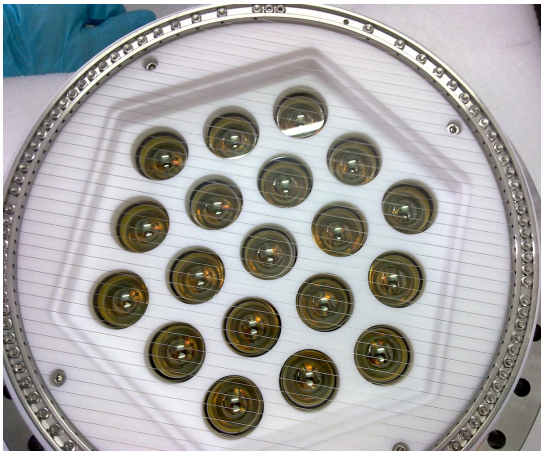

Figure 4.6: The energy plane of NEXT-DEMO, equipped with 19 Hamamatsu R7378A PMTs.

The energy plane (see Figure 4.6) is equipped with 19 Hamamatsu R7378A photomultiplier tubes. These are 1-inch, pressure-resistant (up to 20 bar) PMTs with acceptable quantum efficiency ($\sim 15\%$) in the VUV region. The resulting photocathode coverage of the energy plane is about 39%. The PMTs are inserted into a PTFE holder following a hexagonal pattern. A grid, known as *shield* and similar to the cathode but with the wires spaced 0.5 cm apart, is screwed on top of the holder and set to electrical ground. As explained above, this protects the PMTs from the high-voltage set in the cathode, and ensures that the electric field in the 10-cm buffer region is below the EL threshold.

The initial operation of NEXT-DEMO implemented a tracking plane made of 19 pressure-resistant photomultipliers, identical to those used in the energy plane but operated at a lower gain. Instrumenting the tracking plane with PMTs during this period simplified the initial commissioning, debugging and operation of the detector due to the smaller number of readout channels (19 PMTs in contrast to the 256 SiPMs currently operating in SiPM tracking plane) and their intrinsic sensitivity to the UV light emitted by xenon. Since October 2012, NEXT-DEMO has been operating with a full tracking plane made with SiPMs, as shown in Figure 4.7.

Figure 4.8 shows the measured energy spectrum of 511-keV gamma rays from ^{22}Na in the fiducial volume of NEXT-DEMO. A gaussian fit to the photoelectric peak indicates an energy resolution of 1.75% FWHM. Extrapolating the result to the Q value of ^{136}Xe (2458 keV) assuming a $E^{-1/2}$ dependence, we obtain a resolution of 0.7% FWHM, better than the NEXT target resolution of 1% FWHM at $Q_{\beta\beta}$. Notice that, unlike the NEXT-DBDM prototype, the DEMO apparatus measures electrons in a large fiducial volume, and therefore this result can be safely extrapolated to NEXT-100. We believe that an ultimate resolution of 0.5% FWHM, as found by DBDM, can eventually be attained.

Figure 4.9 shows an electron produced by photoelectric interactions of the 511-keV gamma rays emitted from a ^{22}Na source. The color code shows the amount of energy deposition. The four pictures show the 3D image and the corresponding three projections.

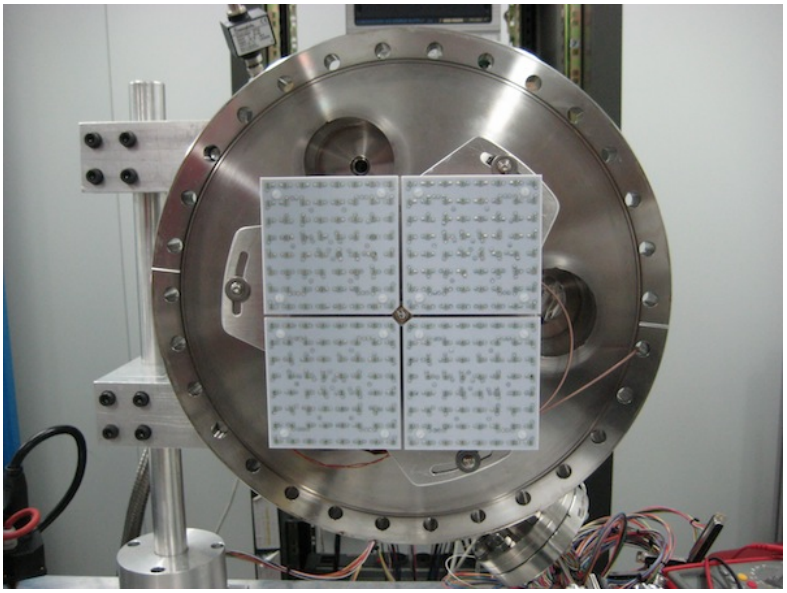

Figure 4.7: Dice Boards installed in NEXT-DEMO, containing 64 (8×8) MPPCs. There will be about 100 such boards in NEXT-100.

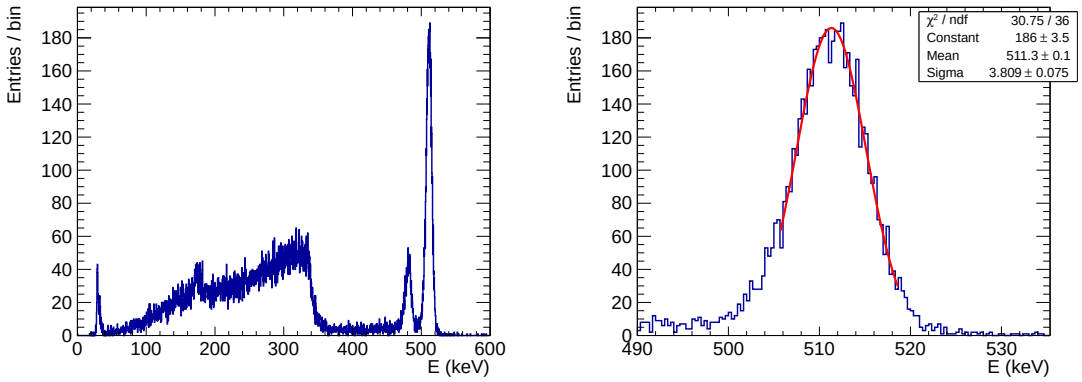

Figure 4.8: Energy spectra for ^{22}Na gamma-ray events within the fiducial volume of NEXT-DEMO. Left: the whole spectrum. Right: zoom in the photoelectric peak.

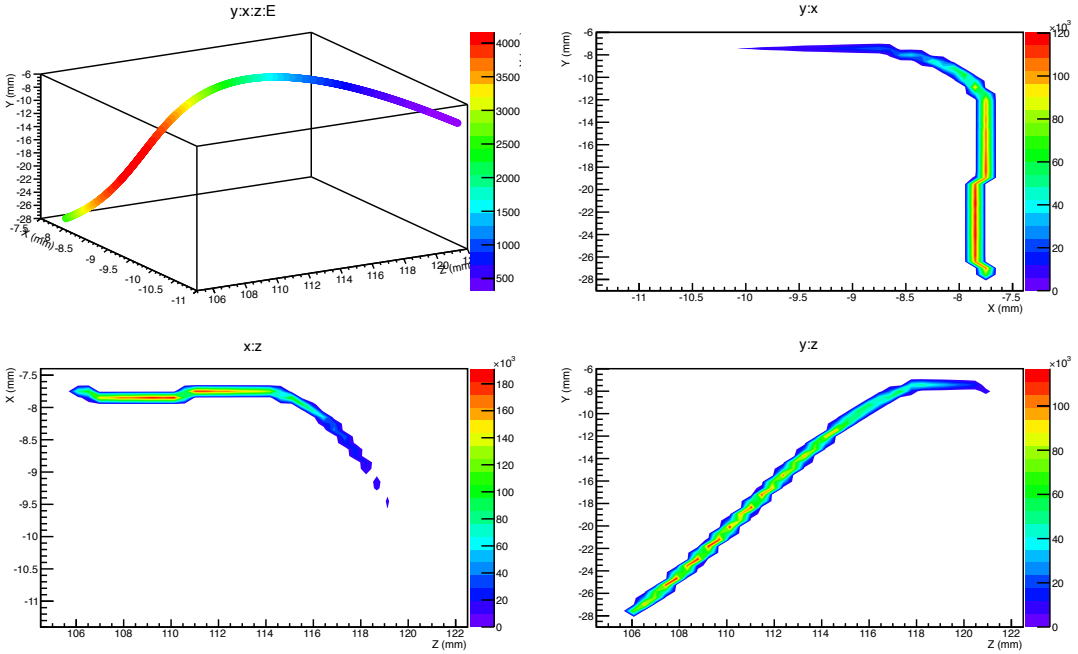

Figure 4.9: An electron produced by a photoelectric interaction of a 511 keV gamma source, reconstructed in the NEXT-DEMO detector.

The presence of a blob is clearly seen, that is a large energy deposition localized in a small volume within the xenon gas, corresponding to the region where electrons range out. Notice that the extension of the blob is large compared with the size of the track. The PMT plane is used to reconstruct the blob energy and the blob position along the drift (z) direction, while the SiPM plane is used to reconstruct the blob position in the (x,y) plane.

Figure 4.10 shows a longer electron produced by photoelectric interactions of the 660-keV gamma rays emitted from a ^{137}Cs source. In both ^{22}Na and ^{137}Cs sources, a single blob of energy deposition is clearly seen, illustrating the power of the topological signature.

Finally, figure 4.11 shows a crossing muon, reconstructed in the NEXT-DEMO detector. Delta rays are observed, but there is no blob at the end.

NEXT-DEMO has been running successfully for two years, proving perfect high voltage operation and a great stability against sparks. The gas system, completed with a hot getter, has demonstrated to be leakproof (less than 0.005 bar leakage per day) and has allowed a continuous recirculation and purification of the gas, which resulted in a measured electron lifetime of only a few milliseconds. The light collection efficiency has been thoroughly understood, by studies of both primary and electroluminescent scintillation signals. The TPB coating on the PTFE reflectors in the drift region produced an increase in the EL light collection of a factor of 3 [35], thus improving light statistics.

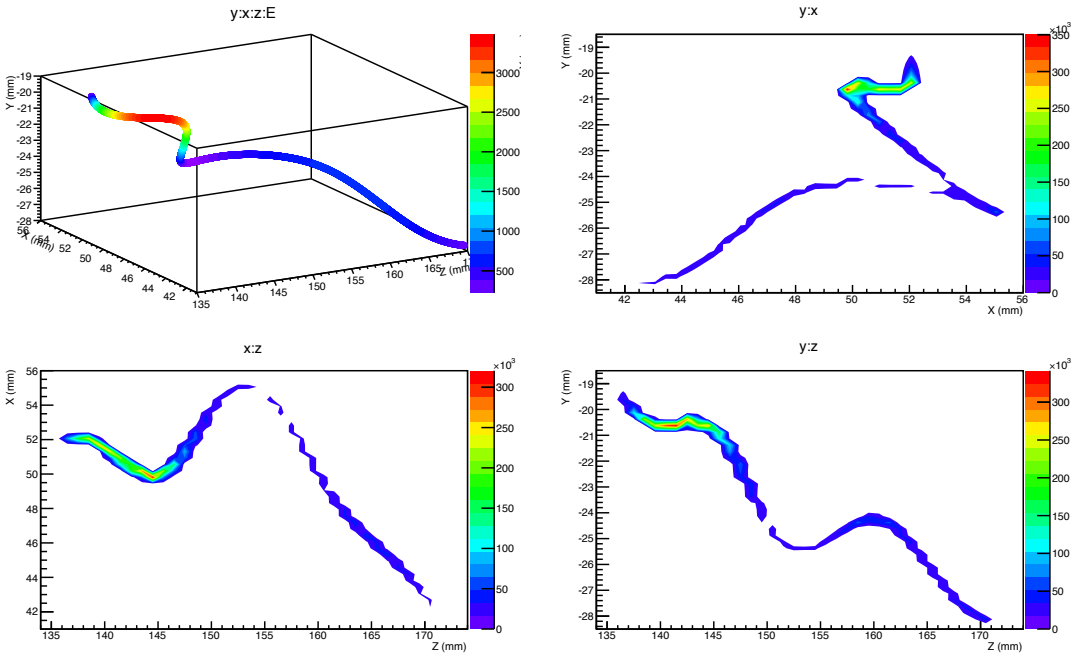

Figure 4.10: An electron produced by a photoelectric interaction of a 660 keV gamma source, reconstructed in the NEXT-DEMO detector.

Data produced with an alpha source have allowed studies of primary scintillation signals along the whole drift length, leading to a better understanding of light reflectance and loss in our detector, through the support of Monte Carlo simulations [33] .

To summarise, the NEXT-DEMO detector, is operating continuously at IFIC since 2011. The current configuration, with a SiPM tracking plane, a PMT energy plane and a light tube coated with TPB, demonstrates the design chosen for the NEXT-100 detector, exercises all the technical solutions, and shows excellent energy resolution and electron reconstruction. Further work is currently in progress analysing the many millions of events acquired with the chamber. NEXT-DEMO is the only detector of its type currently operating in the world.

4.3 NEXT-DBDM

The basic building blocks of the NEXT-DBDM xenon electroluminescent TPC shown in figures 4.13 and 4.12 are: a stainless steel pressure vessel, a gas system that recirculates and purifies the xenon at 10-15 atm, stainless steel wire meshes that establish high-voltage equipotential planes in the boundaries of the drift and the EL regions, field cages with hexagonal cross sections to establish uniform electric fields in those regions, an hexagonal pattern array of 19 VUV sensitive PMTs inside the pressure vessel and an associated readout electronics and data acquisition (DAQ) system.

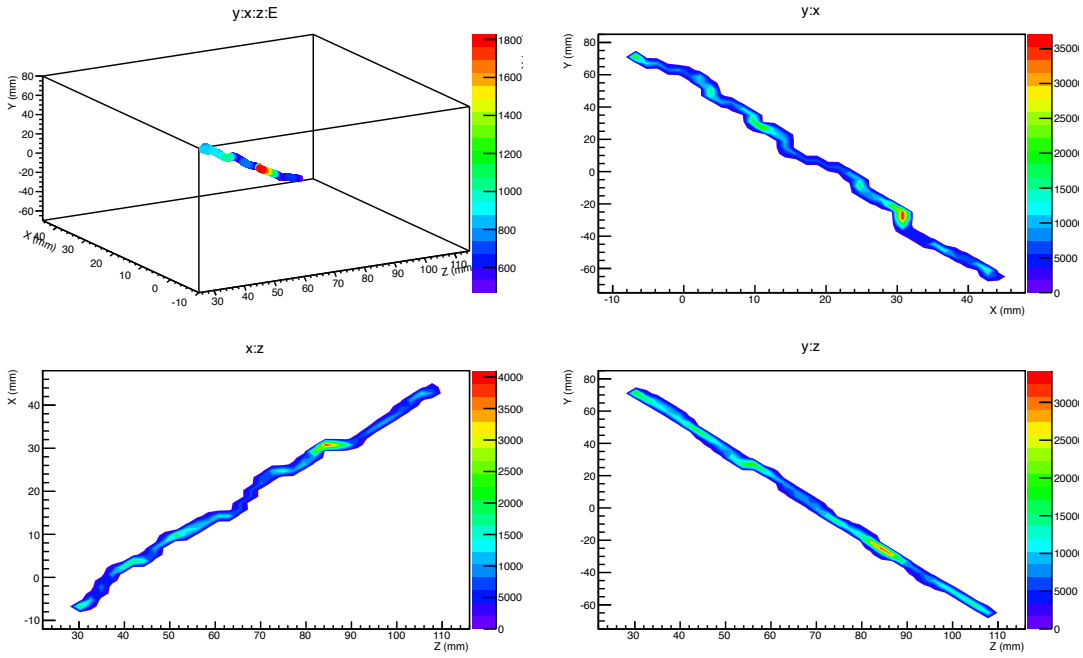

Figure 4.11: A crossing muon, reconstructed in the NEXT-DEMO detector. Delta rays are observed, but there is no blob at the end.

In the NEXT-DBDM detector the PMT array and the EL region, which are both hexagonal areas with 12.4 cm between opposite sides, are 13.5 cm away from each other (see Fig.4.12). Thus point-like isotropic light produced in the EL region illuminates the PMT array with little PMT-to-PMT variation. This geometric configuration also makes the illumination pattern and the total light collection only very mildly dependent on the position of the light origin within the EL region. The diffuse reflectivity of the TPC walls increases this light collection uniformity further. As a result, the device provides good energy measurements with little dependence on the position of the charge depositions. On the other hand, without a light sensor array near the EL region precise tracking information is not available and only coarse average position can be obtained using the PMT array light pattern.

The field configuration in the TPC is established by five stainless steel meshes with 88% open area at a z position of 0.5 cm (cathode buffer or PMT mesh), 5.5 cm (cathode or drift start mesh), 13.5 cm (field transition or EL-start mesh), 14.0 cm (anode or EL-end mesh) and 19.0 cm (anode buffer or ground mesh) from the PMT windows. Electroluminescence occurs between 13.5 and 14.0 cm. The meshes are supported and kept tense by stainless steel frames made out of two parts and tensioning screws on the perimeter. The TPC side walls, made out of 18 individual rectangular assemblies 7.1 cm wide (and 5 and 8 cm length) connecting adjacent meshes (except around the 0.5 cm EL gap), serve the dual purpose of light cage and field cage. Each side wall assembly is made

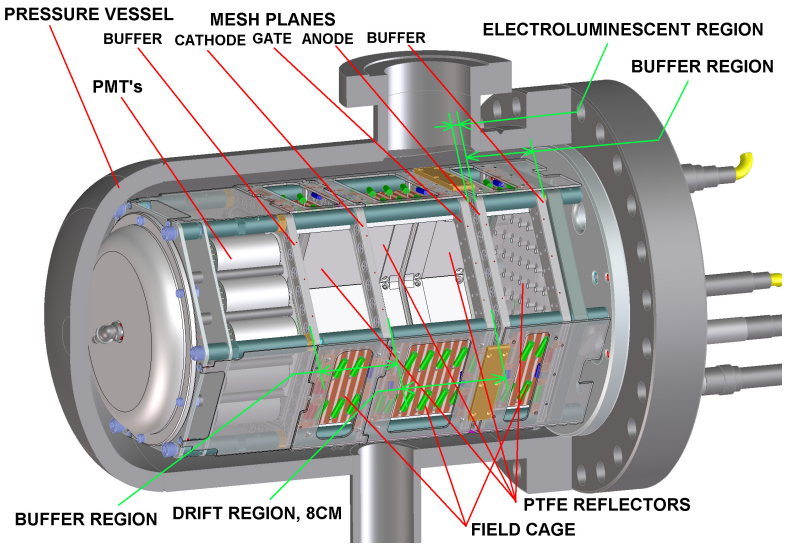

Figure 4.12: **NEXT-DBDM electroluminescent TPC configuration:** An array of 19 photomultipliers (PMTs) measures S1 primary scintillation light from the 8 cm long drift region and S2 light produced in the 0.5 cm electroluminescence (EL) region 13.5 cm away from the PMTs. Two 5 cm long buffer regions behind the EL anode mesh and between the PMTs and the cathode mesh grade the high voltages (up to $\pm$17 kV) down to ground potential.

of a 0.6 cm thick PTFE panel and a ceramic support panel. The PTFE panels are bare on the side facing the active volume and have copper stripes parallel to the mesh planes every 0.6 cm on the other side. The bare PTFE serves as reflector for the VUV light. Adjacent copper stripes are linked with 100 MΩ resistors to grade the potential and produce a uniform electric field. The ceramic support panels are connected, mechanically and electrically, to the outer perimeter of the mesh support frames and to the first and last copper stripes on their corresponding PTFE panel. High voltage connections to establish the TPC fields (HHV) are made directly to the mesh frames.

The NEXT-DBDM TPC configuration with the PMT array 13.5 cm from the EL region does not permit detailed track reconstruction in the $x-y$ plane. Still, the position reconstruction achievable allows the fiducialization of pulses to select events/pulses within regions of the TPC with uniform light collection efficiencies. The position reconstruction for isolated 50-100 keV energy depositions displays the hexagonal boundary of the TPC. A scaling factor of $\sim$30 and an $x-y$ offset are needed to convert charge-weighted average x and y positions to true TPC (x, y) coordinates.

In Fig. 4.14 the energy spectrum in the 662 keV full energy region obtained at 10 atm is shown. A 1.1% FWHM energy resolution was obtained for events reconstructed in the central 0.6 cm radius region. A small drift-time dependent correction for attachment losses with $\tau = 13.9$ ms was applied. The xenon X-ray escape peak is clearly visible $\sim$30 keV below the main peak. For the spectrum taken at 15 atm a 1% FWHM resolution

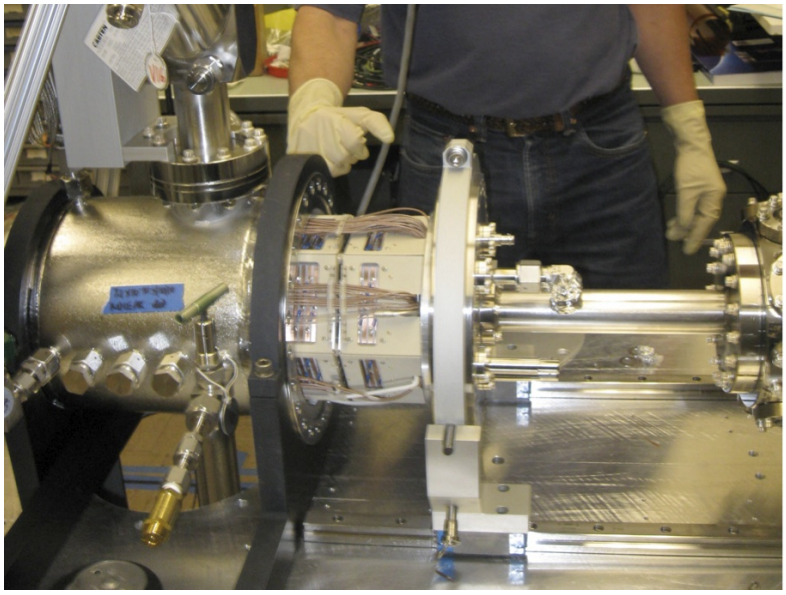

Figure 4.13: The NEXT-DBDM prototype, operating at LBNL. Insertion of the time projection chamber into the stainless-steel pressure vessel.

was obtained. This resolution extrapolates to 0.52% FWHM at $Q_{\beta\beta}$=2.459 MeV if the scaling follows a statistical $1/\sqrt{E}$ dependence and no other systematic effect dominates.

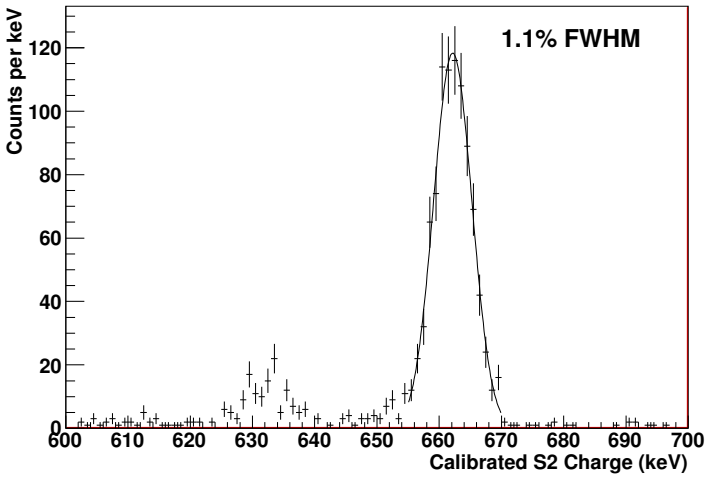

Figure 4.14: **Energy resolution at 10 atm for 662 keV gamma rays:** These data were taken at 10.1 atm with a 0.16 kV/cm field in the drift region and 2.08 kV/(cm atm) in the EL region. If assumed to follow a $1/\sqrt{N}$ dependence this resolution extrapolates to 0.57% at $Q_{\beta\beta}$=2.459 MeV.

In order to study the EL TPC energy resolution at lower energies, full energy 662 keV events that had a well separated X-ray pulse reconstructed in the central 1.5 cm radius region were used. The energy calibration was done on the 662 keV full energy peak and linearity with a zero intersect was assumed. Figure 4.15 shows the energy spectrum obtained at 10 atm with a 5% FWHM resolution. The spectrum was fit to the sum of four gaussians with relative positions and intensities fixed to the strongest xenon X-ray lines. The absolute position of the anchor peak and the peaks' widths (all assumed the same) were obtained from the fit. The anchor peak is at 29.1 keV, less than 2% away from its nominal 29.6 keV value.

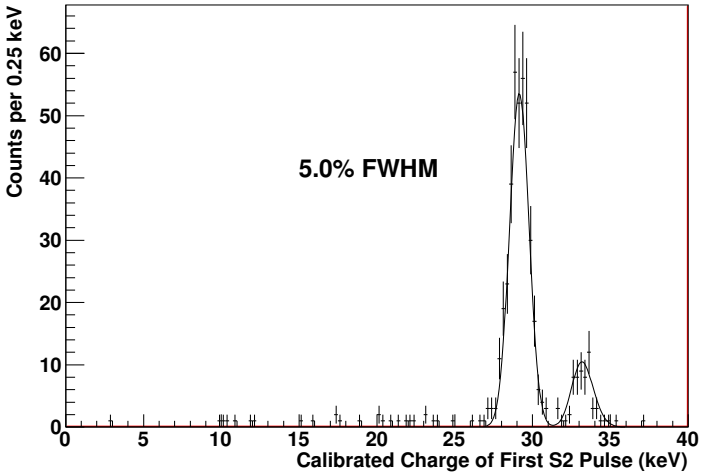

Figure 4.15: **Energy resolution at 10 atm for 30 keV xenon X-rays:** A 5% FWHM energy resolution for 30 keV was obtained. These data were taken at 10.1 atm with a 1.03 kV/cm field in the drift region and 2.68 kV/(cm atm) in the EL region.

Figure 4.16 summarizes our measurements and understanding of the EL TPC energy resolution. The lower diagonal line represents the Poisson statistical limit from the measurement of a small fraction of the photons produced by the EL gain while the upper diagonal line includes the degradation (mostly from PMT afterpulsing) due to PMT response. The circle data points show the energy resolutions obtained for dedicated LED runs with varying light intensities per LED pulse. The LED points follow the expected resolution over the two decades range studied. The two horizontal lines represent the xenon gas nominal intrinsic resolution for 30 and 662 keV, respectively, and the two curved lines are the expected EL TPC resolutions with contributions from the intrinsic limit and the photons' measurement. Our 662 keV data (squares) and xenon X-ray data (triangles) taken with various EL gains follow the expected functional form of the resolution but are 20-30% larger possibly due to the $x - y$ response non-uniformity. Detailed track imaging from a dense photosensor array near the EL region, such as the one recently commissioned for the NEXT-DBDM prototype (see below), will enable the

application of $x - y$ position corrections to further improve the energy measurement.

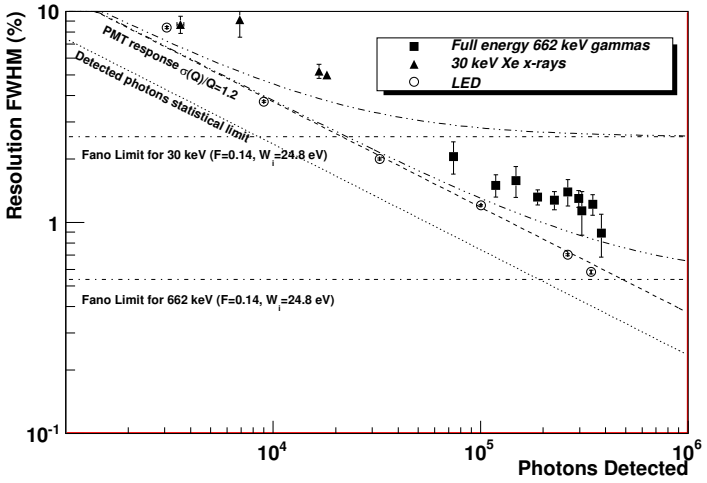

Figure 4.16: **Energy resolution in the high-pressure xenon NEXT-DBDM electroluminescent TPC:** Data points show the measured energy resolution for 662 keV gammas (squares), ∼30 keV xenon X-rays (triangles) and LED light pulses (circles) as a function of the number of photons detected. The expected resolution including the intrinsic Fano factor, the statistical fluctuations in the number of detected photons and the PMT charge measurement variance is shown for X-rays (dot dot dashed) and for 662 keV gammas (dot dot dot dashed). Resolutions for the 662 keV peak were obtained from 15.1 atm data runs while X-ray resolutions we obtained from 10.1 atm runs.

Part II

Project management and finances

Chapter 5

Project Management Plan

5.1 Introduction

The NEXT Project Management Plan (PMP) coordinates the construction of the NEXT-100 detector. It is under the direct supervision of the Spokesperson (IP) and the Project Manager (PM). The PM of NEXT is Dr. I. Liubarsky, part of the IFIC group.

The PMP follows the progress of each NEXT project, monitors deliverables and deadlines and keeps track of the invested resources including personnel. It also identifies potential problems, synergies and possible conflicts between the different projects and optimizes the sharing of resources.

Figure 5.1 illustrates the overall project concept:

- The project hangs from the top row which has been fully completed in 2012. NEXT prototypes have demonstrated the physics performance (resolution, tracking) and validate the technology (choice of EL SOFT TPC). The screening campaign allows the selection of radiopure components and defines the background model. At the same time, the detector design has been completed, with a full specification of solutions for mechanics and electronics as well as the choice of sensors.
- Construction of the detector and completion of software tools (already developed for prototypes) happens during 2013 (phase 1 construction) and 2014 (phase 2 construction).
- Detector commissioning with natural xenon (NXE) is foreseen by 2014.
- Physics run with enriched xenon (EXE) is foreseen in 2015.

5.2 Working Packages

The PMP is structured in terms of Working Packages (WP). Figure 5.2 shows the 15 WPs that form the PMP and their dependences. In the following subsections we summarise the main WP and their time lines (Gantt charts).

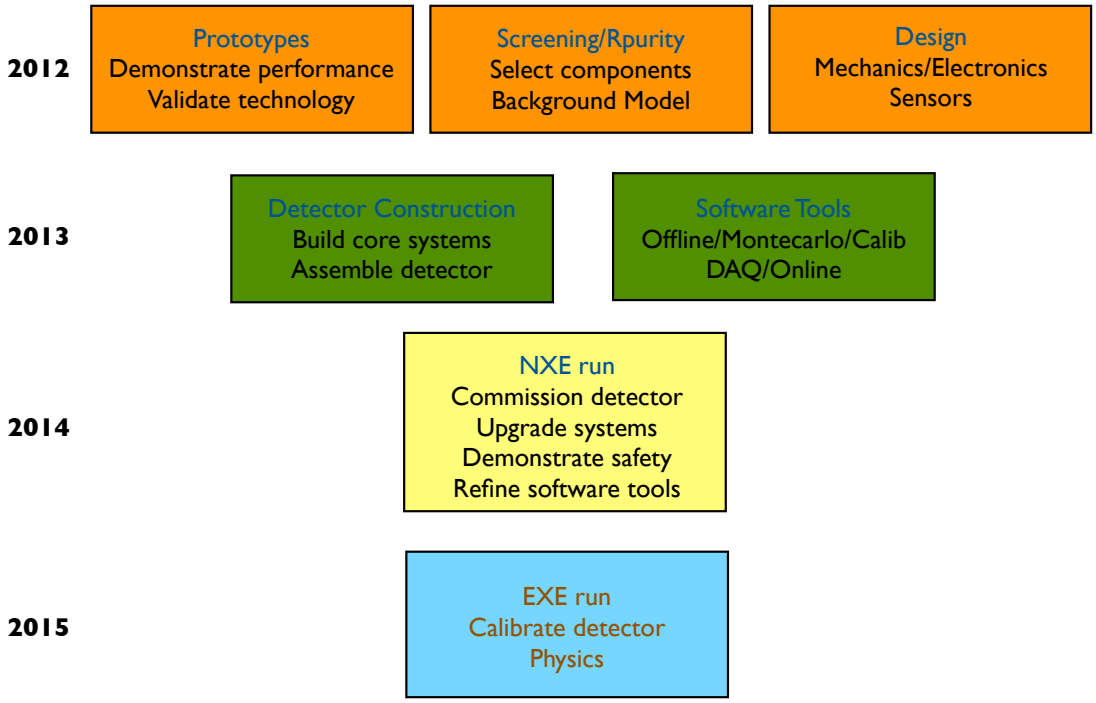

Figure 5.1: The overall project concept.

Figure 5.3 shows the time line development of WP0 (Detector), illustrating the overall development of the project. Notice that the time line for WP0 is computed automatically in the Gantt chart from the time lines of all the other projects. For each project, the stages marked on green have already been accomplished.

5.2.1 WP0: Detector

- **Goal:** detector commissioning, calibration and physics run.
- **Significant specs:** strong links with the Calibration and Software WP.
- **Main contributors:** IFIC, TAMU, LBNL (coordination).
- **Working Package Manager:** A. Goldschmidt (LBNL).

5.2.2 WP1: Vessel

- **Goal:** construction of the pressure vessel.
- **Significant specs:** built with 316Ti alloy of low activity (∼0.2 mBq/kg for the thorium series and the uranium series, already measured at the LSC by NEXT). Certified to 20 bar, can operate up to 15 bar. Follows ASME norm. Includes an

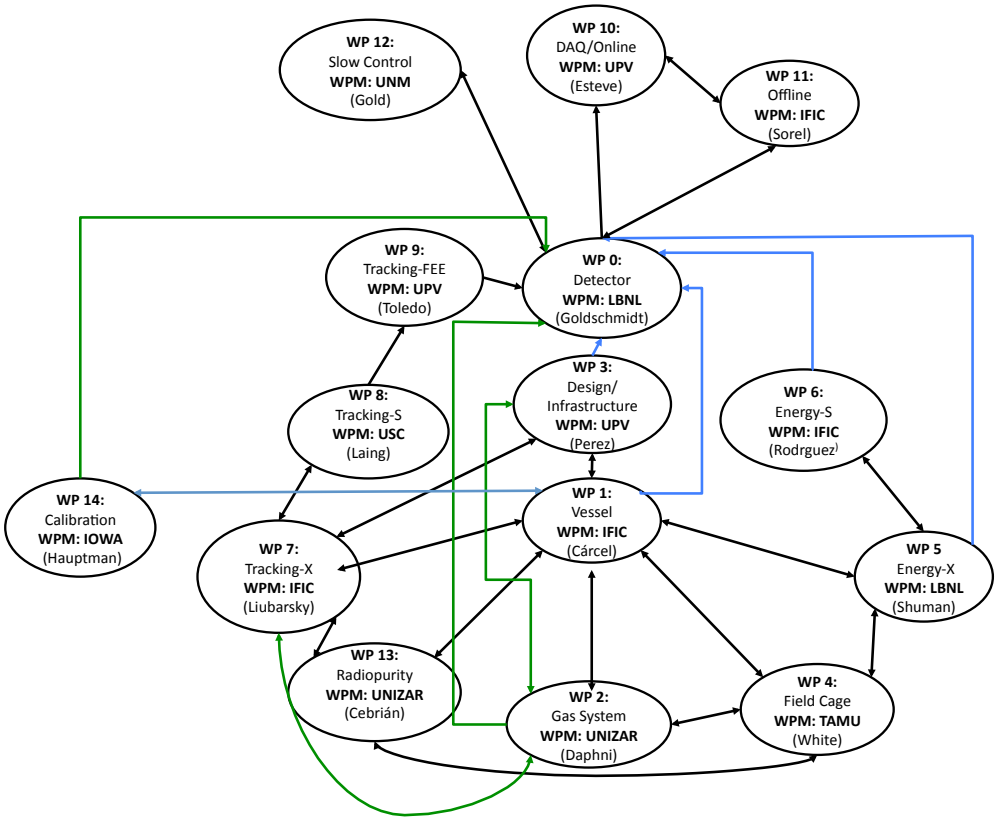

Figure 5.2: Structure of the working packages.

inner copper shield (ICS) made of radiopure copper, with an activity of about 10 μBq/kg.

- **Main contributors:** LBNL (design), IFIC (design, construction, coordination).
- **Working Package Manager:** S. Cárcel (IFIC).

5.2.3 WP2: Gas system

- **Goal:** construction of the gas system.
- **Significant specs:** needs to operate with NXE and EXE. Maximum loss of EXe to atmosphere: 10 g/year.

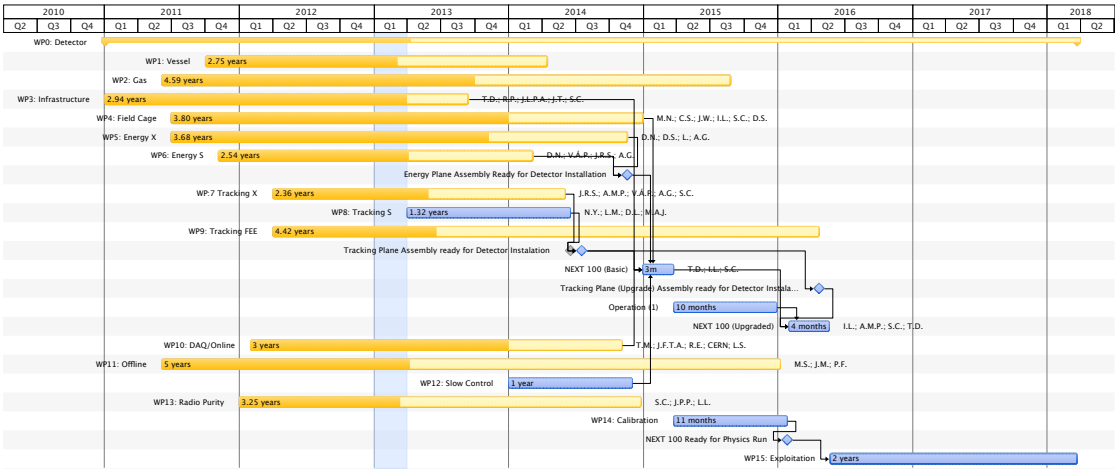

Figure 5.3: WP0 (Detector) time line.

- **Main contributors:** IFIC (design, part procuration), UNIZAR (installation at LSC, coordination).
- **Working Package Manager:** T. Dafni (UNIZAR).

Figure 5.5 shows the time line development of the project. Notice that the gas system goes through two clearly differentiated stages. The basic loop which allows operation with natural xenon (NXe) and is already installed at the LSC, and the advanced loop (which includes a sophisticated pump, as well as safety and recovery systems) which allows operation with enriched xenon (EXe) and is foreseen to start in mid 2014.

5.2.4 WP3: Infrastructures

- **Goal:** construction of the infrastructures needed for NEXT (platform, pedestal, lead castle, etc.). Analysis and design of operational parameters (gas flow, electric fields) in NEXT.
- **Significant specs:** the detector must be independent on the shielding and platform structure, to withstand seismic activity.
- **Main contributors:** UPV (design, coordination), LSC (installation).
- **Working Package Manager:** J.L. Pérez (UPV).

5.2.5 WP4: Field Cage

- **Goal:** construction of the field cage, light tube, HVFT and EL grids.
- **Significant specs:** HVFT and EL grids to follow NEXT-DEMO design.

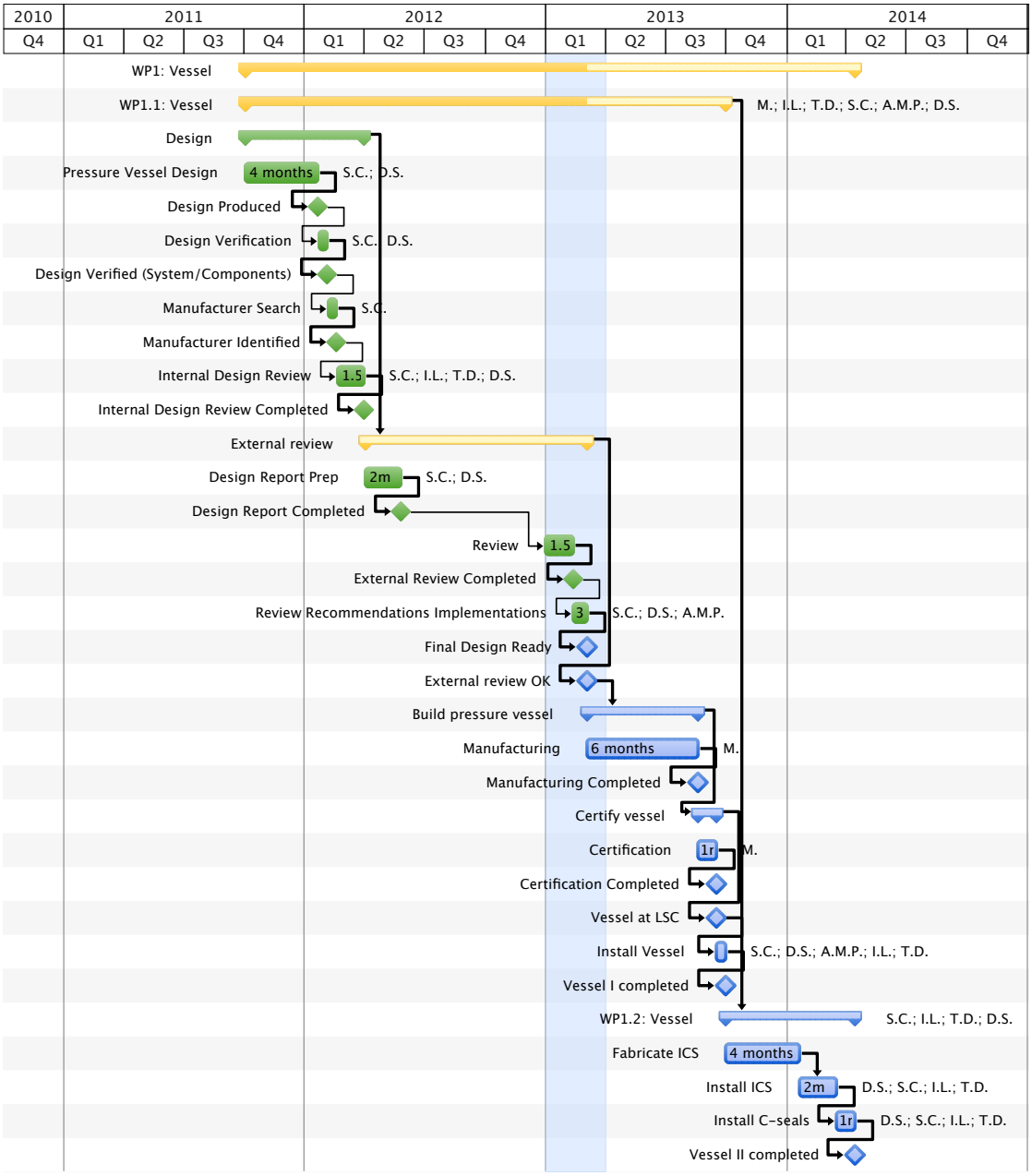

Figure 5.4: WP1 (Vessel) time line.

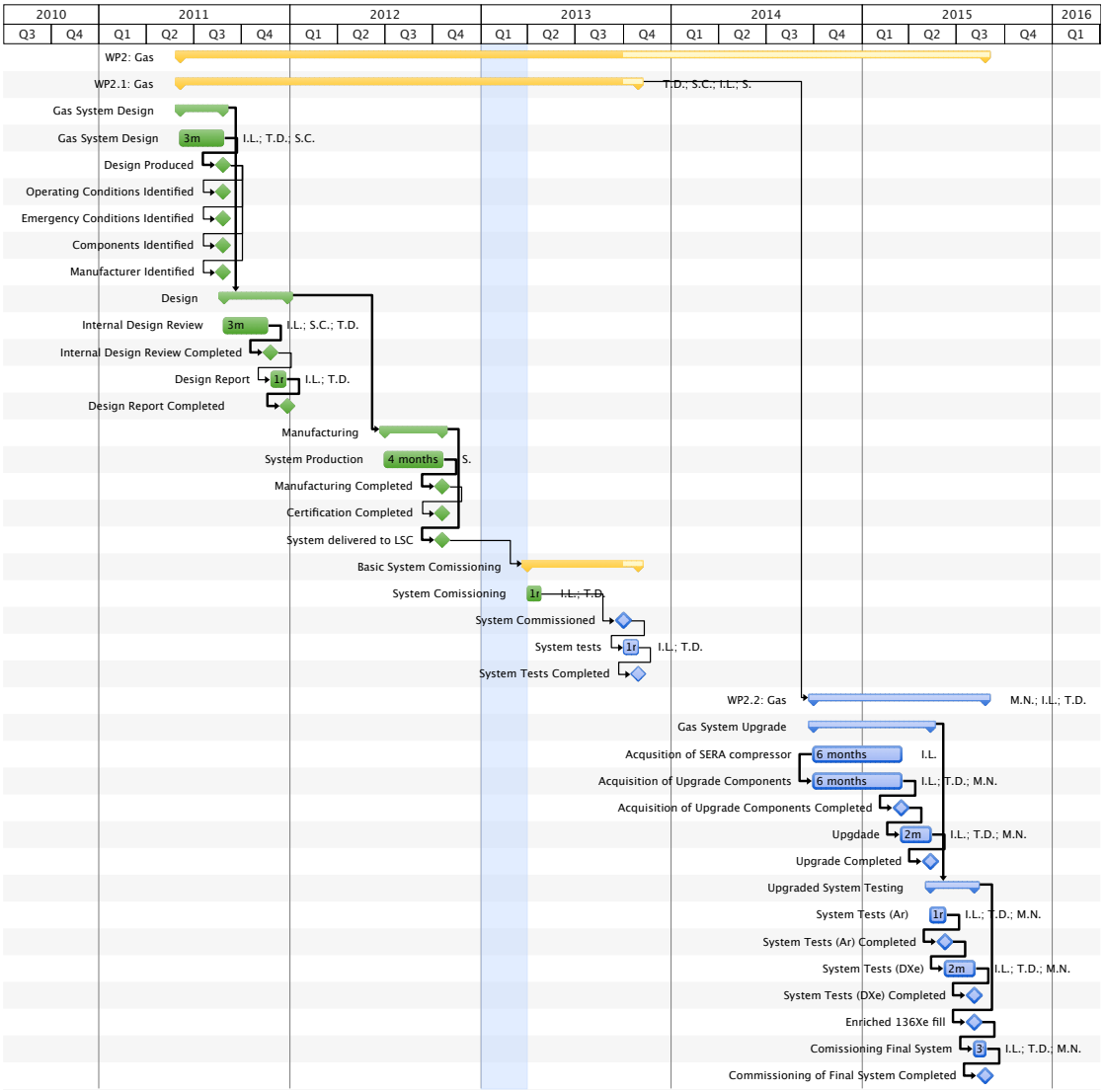

Figure 5.5: WP2 (Gas system) time line.

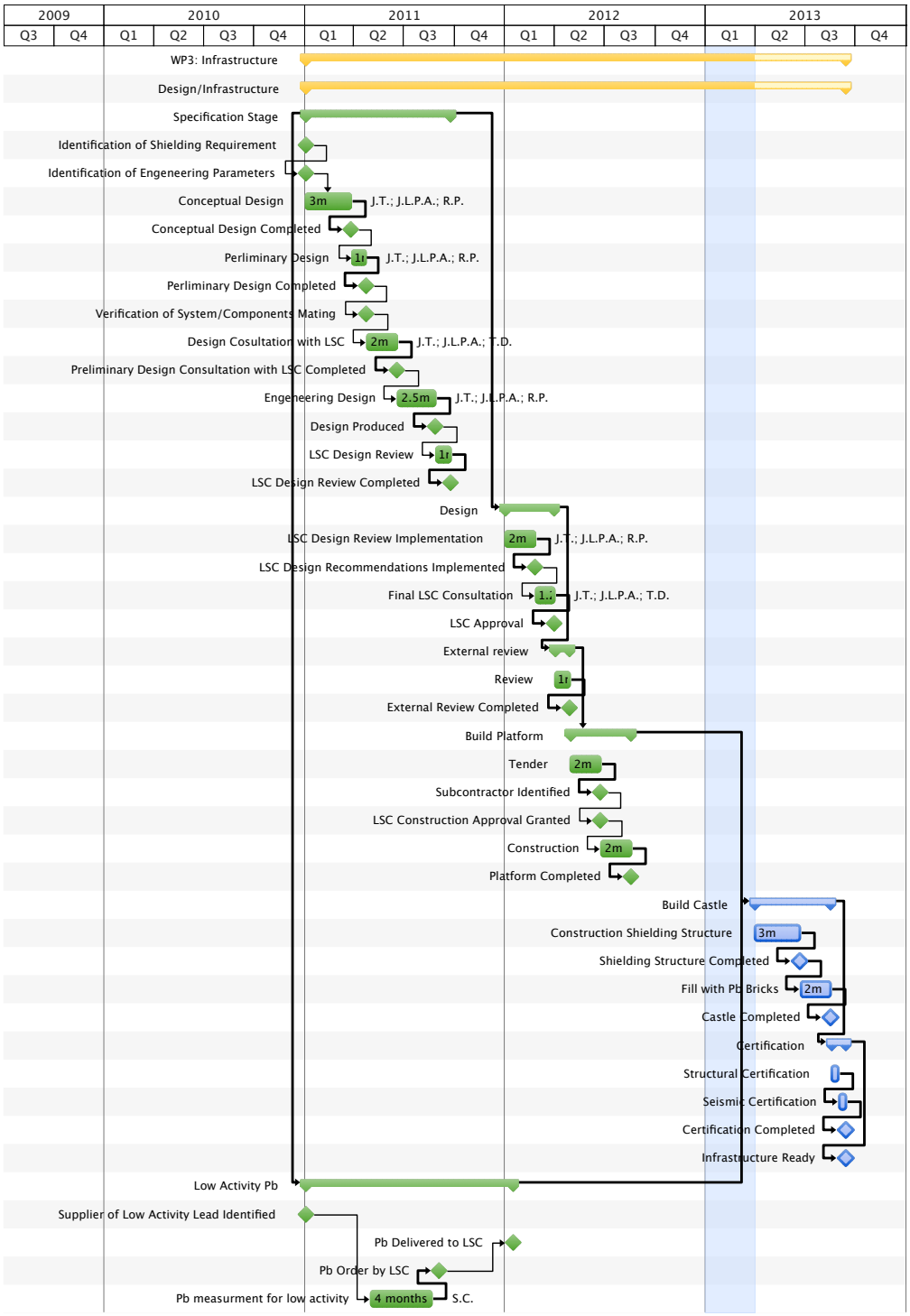

Figure 5.6: WP3 (Infrastructures) time line.

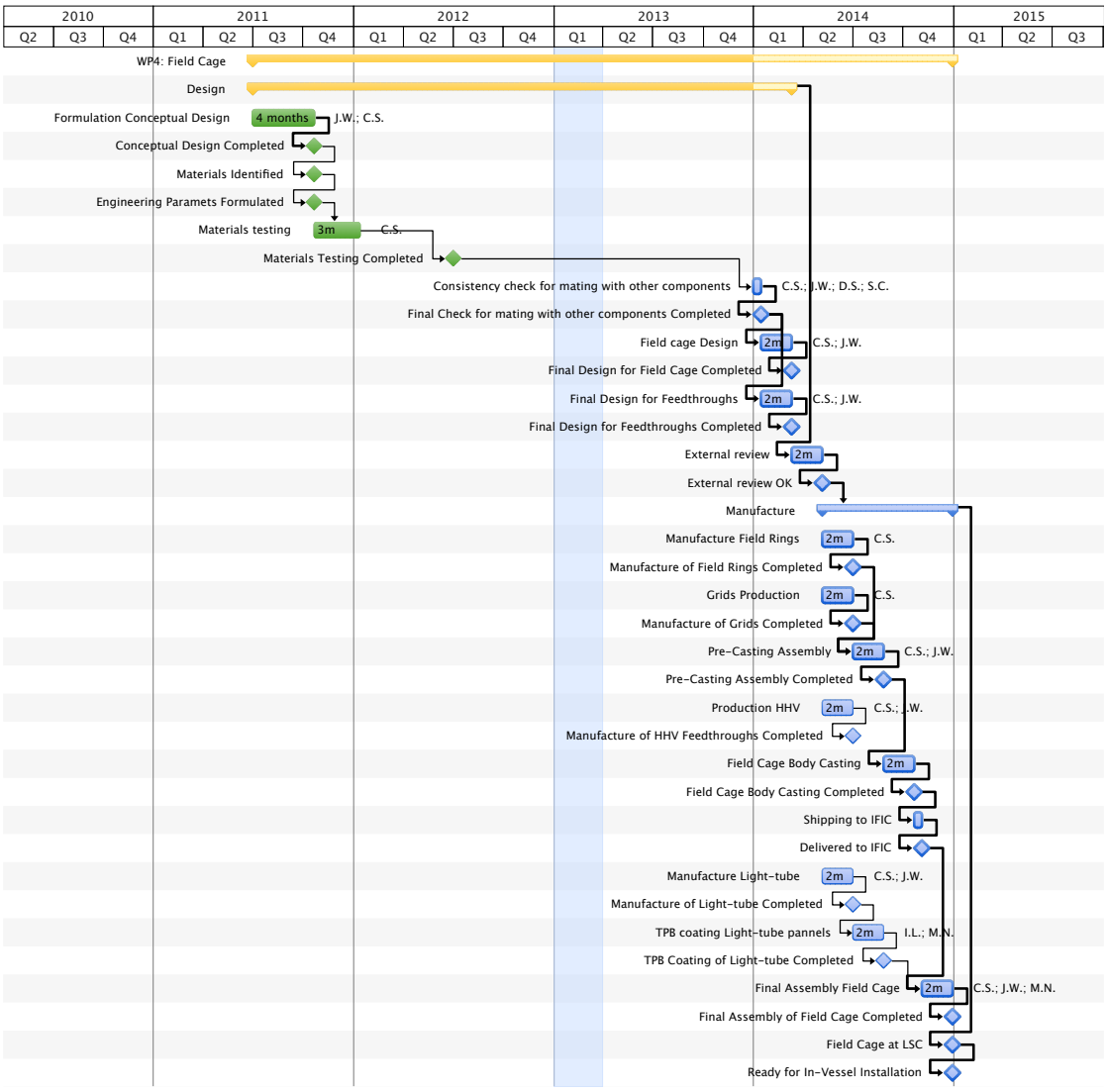

Figure 5.7: WP4 (Field Cage) time line.

- **Main contributors:** TAMU (design, construction, coordination), IFIC (design, TPB coating of light tube).
- **Working Package Manager:** J. White (TAMU).

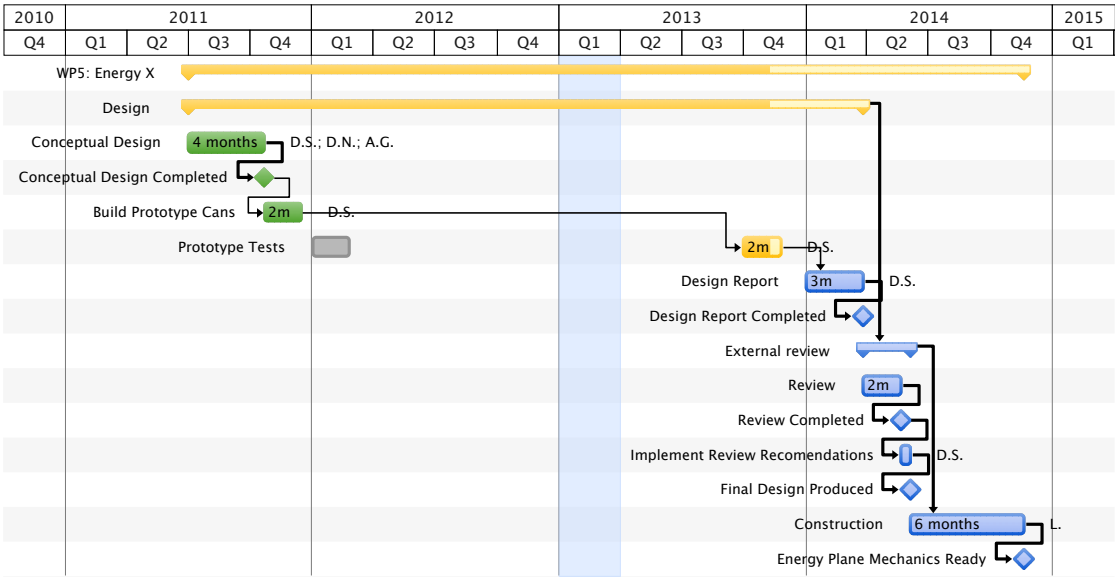

Figure 5.8: WP5 (Infrastructures for the energy plane) time line.

5.2.6 WP5: Energy X

- **Goal:** infrastructures for the energy plane.
- **Significant specs:** PMTs are isolated in individual enclosures connected to a vacuum manifold.
- **Main contributors:** LBNL (design, construction, coordination), IFIC (TPB coating of quartz window).
- **Working Package Manager:** D. Shuman (LBNL).

5.2.7 WP6: Energy S

- **Goal:** sensors and FEE for Energy plane.
- **Significant specs:** PMT bases made of Cirlex or Cuflon for low background. Upgrade to differential output, with the corresponding modifications of bases and FEE.

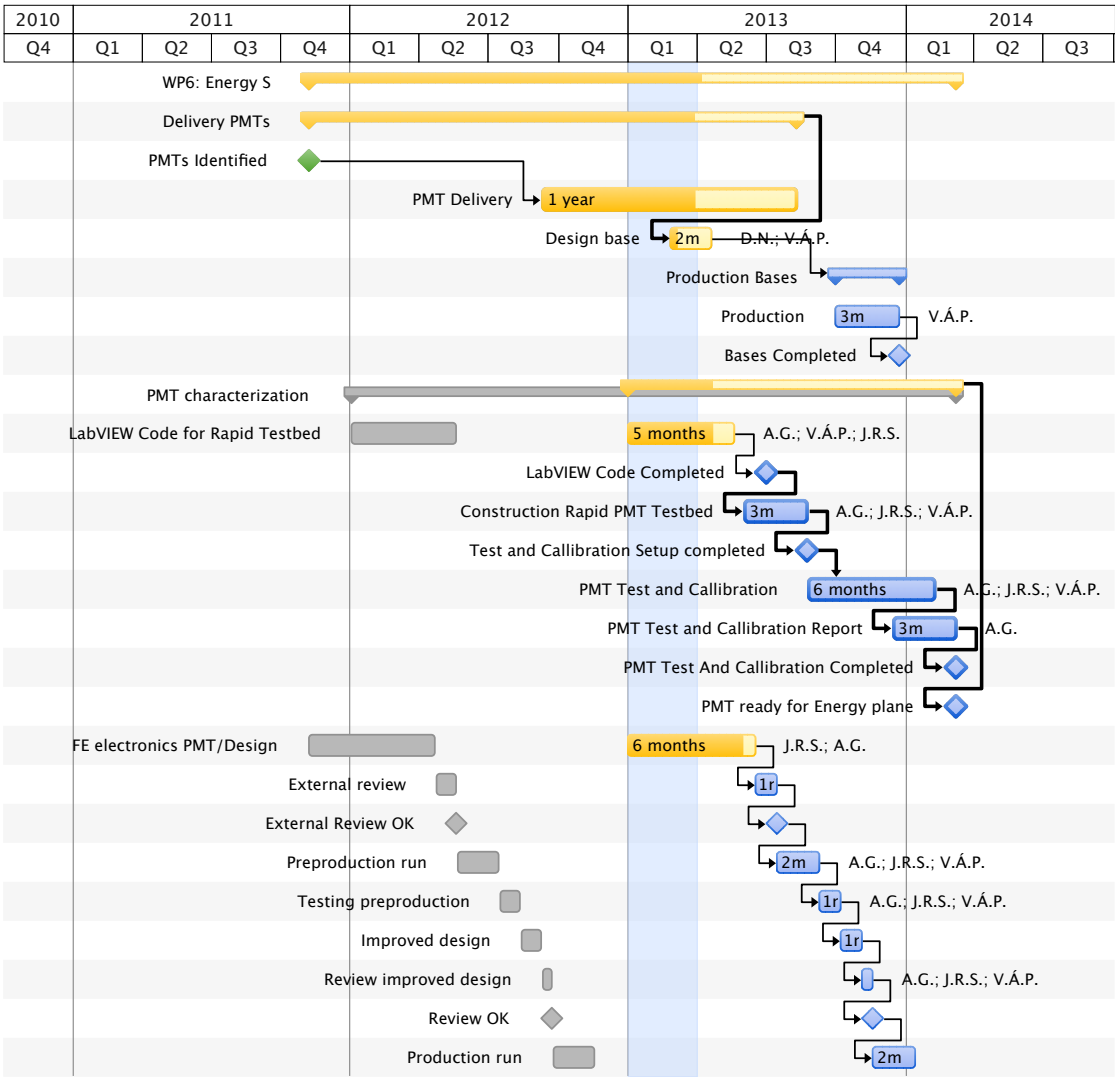

Figure 5.9: WP6 (Sensors and FEE for the energy plane) time line.

- **Main contributors:** IFIC (procurement of sensors, testing, electronics, coordination), Aveiro (testing).
- **Working Package Manager:** J. Rodríguez (IFIC).

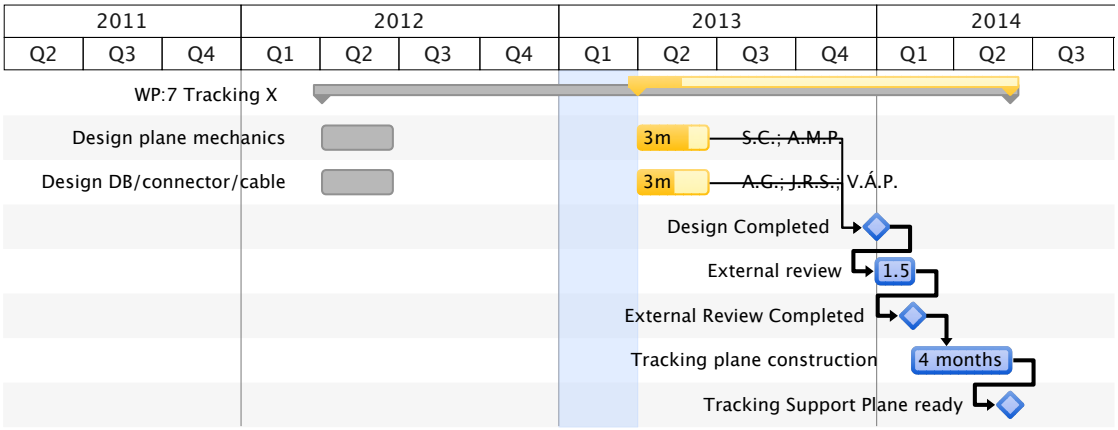

Figure 5.10: WP7 (Infrastructures for the tracking plane) time line.

5.2.8 WP7: Tracking X

- **Goal:** infrastructures for the tracking plane.
- **Significant specs:** DBs made of Cuflon.
- **Main contributors:** IFIC (mechanics, electronics, coordination), LBNL (design).
- **Working Package Manager:** I. Liubarsky (IFIC).

5.2.9 WP8: Tracking S

- **Goal:** tracking sensors, arranged in DBs.
- **Significant specs:** DBs coated with TPB.
- **Main contributors:** IFIC (coordination, construction 1/3 of DB), Coimbra (construction 1/3 of DB), UAN (construction 1/3 of DB).
- **Working Package Manager:** A. Laing (IFIC).

5.2.10 WP9: Tracking-FEE

- **Goal:** front end electronics for the MPPCs.
- **Significant specs:** 7 000 channels, low background, low power.

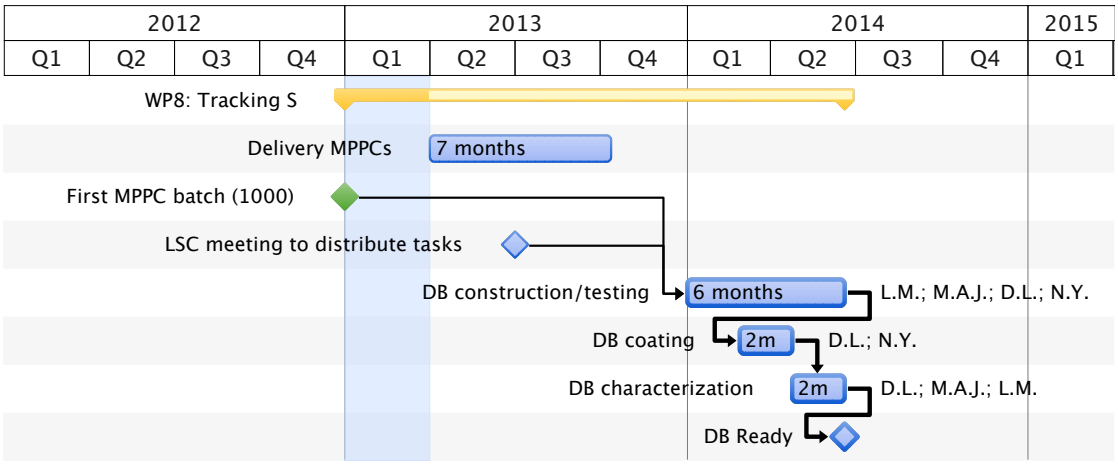

Figure 5.11: WP8 (Sensors for the tracking plane) time line.

- **Main contributors:** UPV (coordination, design), LBNL (design).
- **Working Package Manager:** J.F. Toledo (UPV).

5.2.11 WP10: DAQ and online

- **Goal:** data acquisition and online programs for NEXT.
- **Significant specs:** use RD51 design (CERN standard), design tested on NEXT-DEMO. Online uses DATE (CERN standard).
- **Main contributors:** UPV (coordination, DAQ), IFIC (online).
- **Working Package Manager:** R. Esteve (UPV).

5.2.12 WP11: Offline

- **Goal:** reconstruction programs, software tools and Monte Carlo for NEXT.
- **Significant specs:** use FMWK (originally from NOvA experiment) as reconstruction framework. Use Geant4 toolkit to develop NEXUS (NEXT MC simulation).
- **Main contributors:** IFIC (FMWK, NEXUS, reconstruction), USC (tracking), LBNL (energy, tracking, reconstruction).
- **Working Package Manager:** M. Sorel (IFIC).

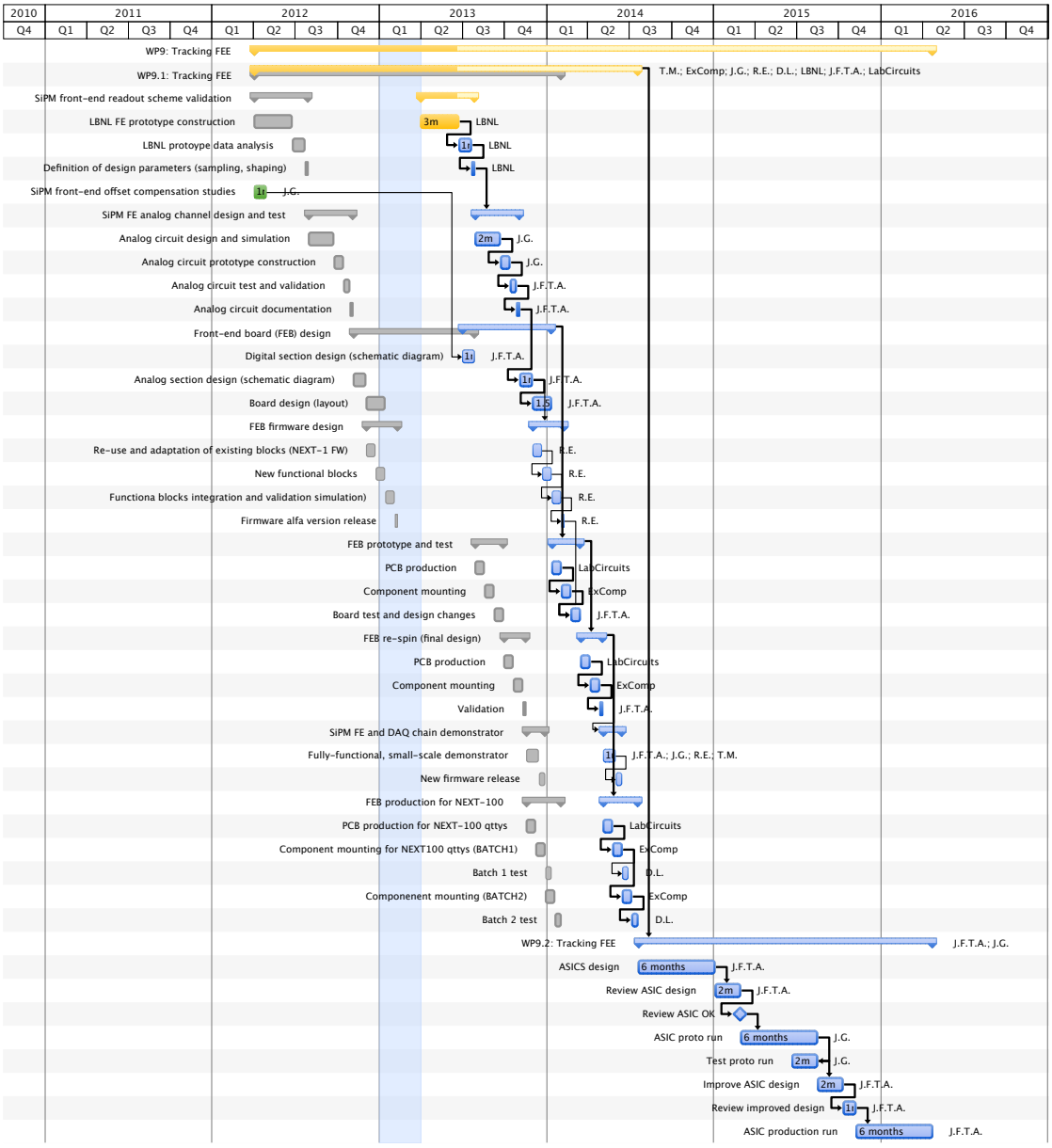

Figure 5.12: WP9 (Front end electronics) time line.

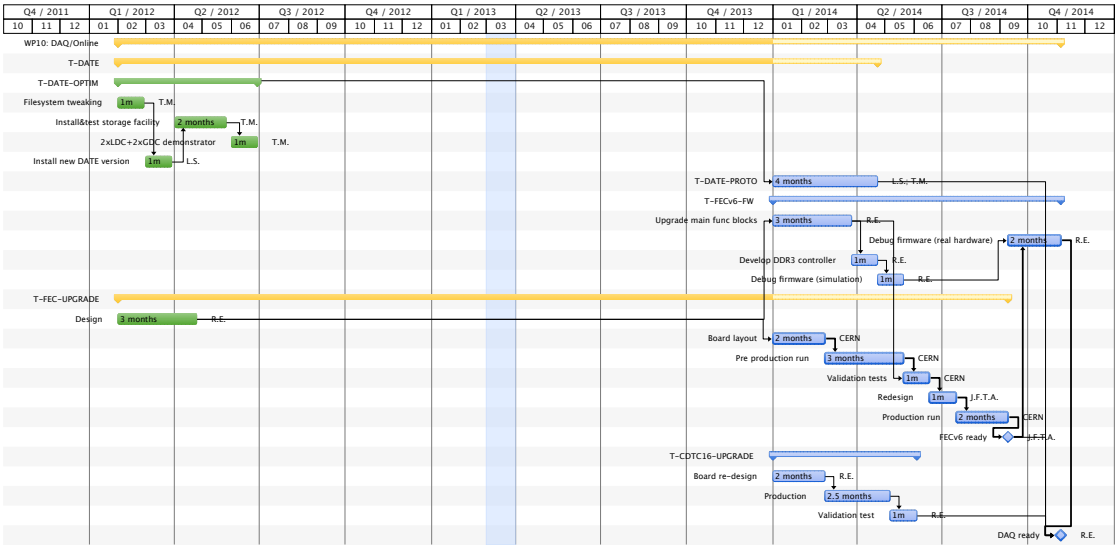

Figure 5.13: WP10 (DAQ and online) time line.

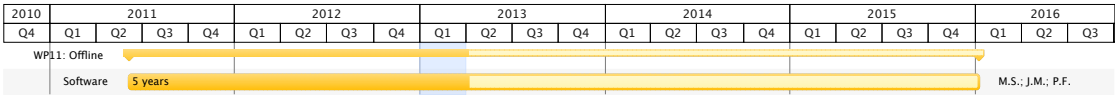

Figure 5.14: WP11 (Offline) time line.

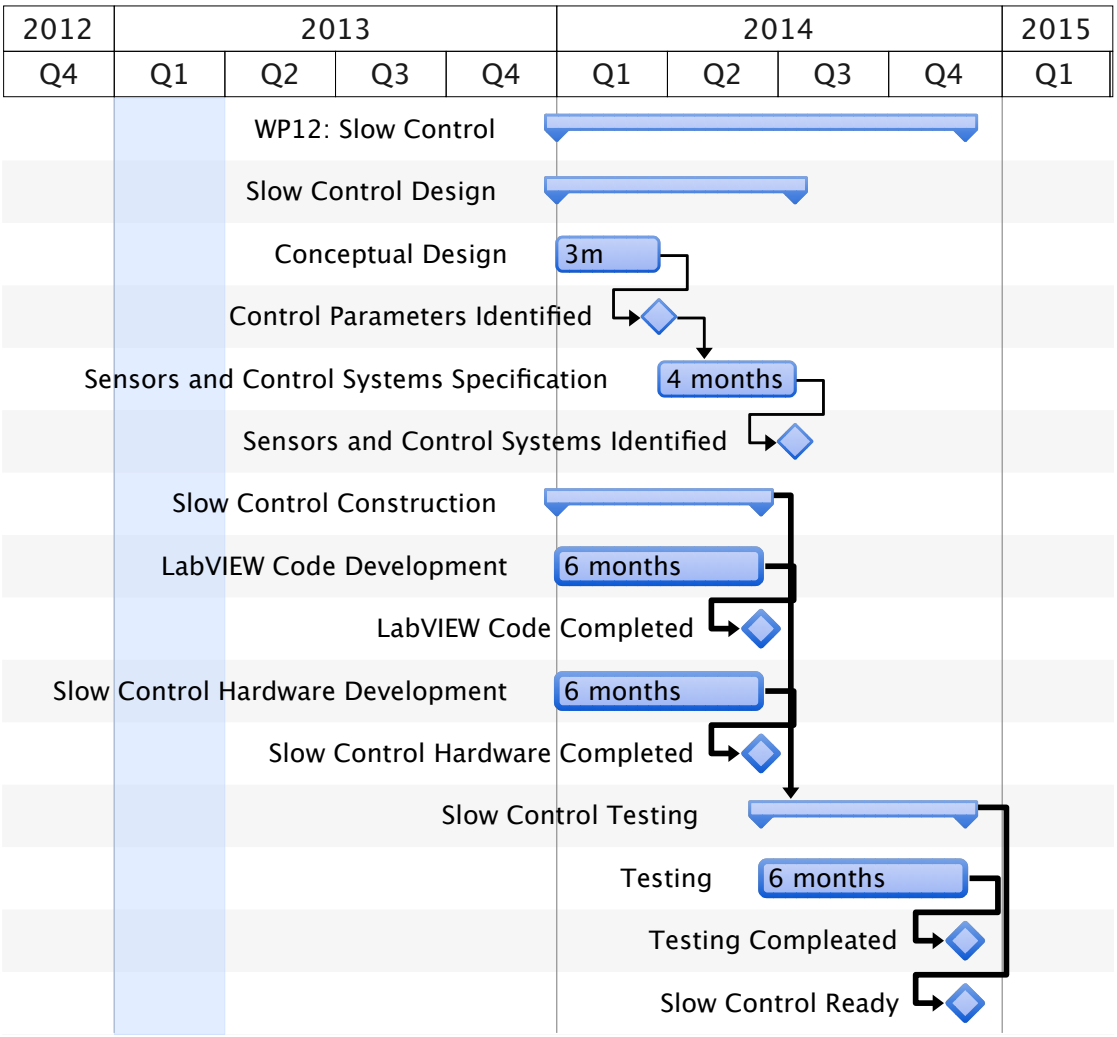

Figure 5.15: WP12 (Slow Controls) time line.

5.2.13 WP12: Slow Controls

- **Goal:** slow control of vital parameters in NEXT (HV, temperature, pressure, gas flow).
- **Significant specs:** follow standards of underground experiments such as XENON.
- **Main contributors:** IFIC, UNIZAR, U. New Mexico.
- **Working Package Manager:** M. Gold (U. New Mexico).

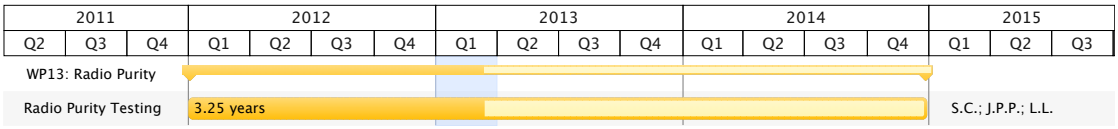

Figure 5.16: WP13 (Radiopurity) time line.

5.2.14 WP13: Radiopurity

- **Goal:** screening of materials for NEXT. Keeps radio-purity data base. Elaborates background model.
- **Significant specs:** extensive use of LSC LBGe detectors.
- **Main contributors:** UAM (screening, data analysis), UNIZAR (coordination).
- **Working Package Manager:** S. Cebrián (UNIZAR).

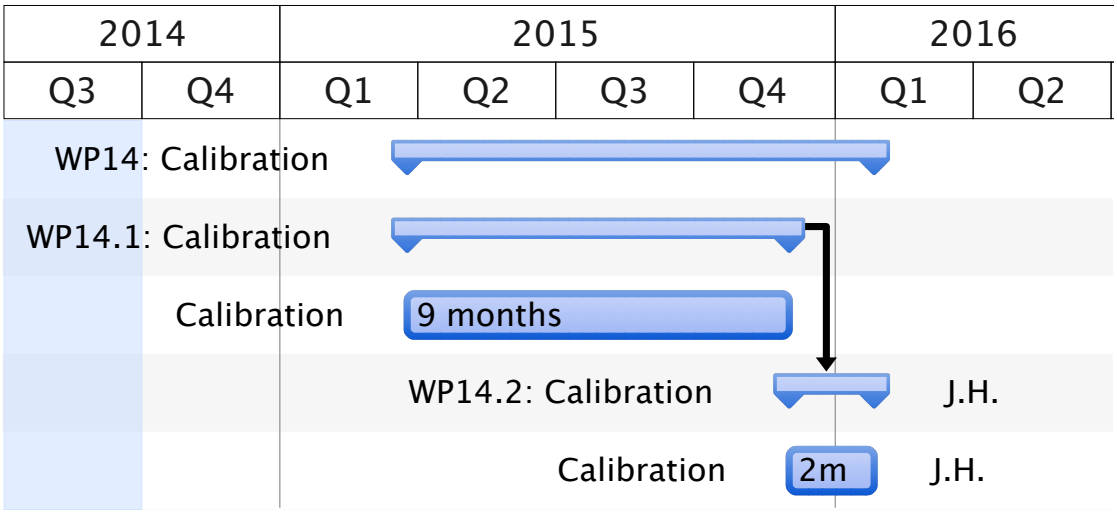

Figure 5.17: WP14 (Calibration) time line.

5.2.15 WP14: Calibration

- **Goal:** Detector calibration with radioactive sources.
- **Significant specs:** Input to hardware design (windows for sources).
- **Main contributors:** IFIC, LBNL (prototypes, data analysis), Iowa (coordination, planning).
- **Working Package Manager:** J. Hauptman (Iowa State).

Chapter 6

NEXT-100 costs

6.1 NEXT costs

In this section we describe the costs associated with the construction, commissioning and operation of the NEXT-100 detector. The construction costs are organised in terms of the working packages (WP) described in the Project Management Plan and refer exclusively to the NEXT-100 detector. The costs associated with the initial phases of the project, including the construction, commissioning and operation of the NEXT-DEMO prototype, are discussed in Chapter 7.

When discussing costs associated to equipment purchase, one has to add to the catalog price of the item three quantities: taxes (e.g., IVA/VAT); overheads charged by universities; and contingency. We thus define the *raw cost* of an item *not yet purchased*, as its catalog price, excluding VAT (e.g, taxes), and without adding contingency and overheads. We define the *direct cost* of an item not yet purchased, as the sum of the raw cost plus taxes plus contingency. Finally, we define the *total cost* of an item not yet purchased as the direct cost plus overheads. In the case of an item *already purchased*, we make no difference between raw cost and total cost.

This distinction is needed to come up with an accurate estimation of the funds needed to complete the construction of the detector. For items already purchased we know exactly the quantity invested, while for items not yet purchased, we typically know the cost without taxes (the tax changes depending on the item and depending on whether we can buy in Spain or elsewhere). Also, for items not yet purchased we need to foresee contingency, which sometimes can be very large (e.g, the cost of ultra pure copper can vary by 50% or more depending on the market within a short period). Adding contingency is essential, since the costs of most items tend to increase with time, but is also ensures a reasonable margin for items with larger taxes, unexpected higher costs, or minor items not contemplated in the budget. Finally, for items not yet purchased we need to foresee overheads (which have already been included in the items purchased), or, alternatively, give the item direct costs, as we will do here.

Table 6.1: Raw costs: WP1 (Pressure Vessel).

Item	**Raw cost**
316Ti Stock	80 000
Vessel Manufacture	45 000
Copper Stock	350 000
Shield Manufacture	40 000
Transportation	2 000
Certification	4 000
TOTAL	**521 000**

6.2 Construction costs

Tables 6.1 to 6.14 detail the raw costs allocated to detector parts and systems organised by WP.

Table 6.15 summarises the raw costs for NEXT construction. Notice that the "travel" items associated with each working group refer to the specific travel for the installation of the system, and do not include additional travel for meetings, commissioning and operation. The total raw costs of the system is € 3 553 890.

In addition to the construction costs, the NEXT experiment requires 100 kg of normal xenon for commissioning and 100 kg of xenon enriched at 90% in the ^{136}Xe isotope for its physics run. The xenon has already been purchased by the LSC and will be borrowed by NEXT. The cost of xenon is M€ 1. Notice that the total cost of the detector, including the enriched xenon, is less than € 5 000 000. This is a rather modest amount compared with other similar experiments. For example, the SuperNemo project, which was considered to operate at LSC before NEXT, has an estimated cost of about € 5 000 000 *per module*, and each module deploys 7 kg of target (to compare with 100 kg in the case of NEXT). Therefore, the ratio scientific output to cost in the case of NEXT is huge.

6.2.1 Cost sharing

Tables 6.16 and 6.17 detail the costs already covered and not yet paid for WP1 (pressure vessel) and WP2 (gas system). CUP funds have been invested to build the pressure vessel and the basic gas loop, with the aim of being able to commission those systems during 2014. The major item not paid for WP1 is the inner copper shield, which is needed only in 2015, when we expect new funds to be available for NEXT. For WP2, the items not yet built are those needed to circulate enriched xenon (the costs are dominated by the hot getters and the compressor), which again, are needed only in 2015.

The costs for WP3 (infrastructures) are assigned to LSC, which provides them as a service. Indeed, it makes sense that items like the working platform or the seismic pedestal built to conform to LSC safety standards, are paid by the laboratory, since those

Table 6.2: Raw costs: WP2 (Gas System).

Item	**Raw cost**
Purification Loop	49 000
Cold Getters	19 000
Re-circulation Compressor	120 000
Hot Getter	80 000
Cold Traps	15 000
Rn Trap	10 000
Emergency Vent Tank	19 000
Multi Channel RGA	17 000
Turbo Vacuum system	20 000
Rough Vacuum pump	7 000
25bar 100mm ID valve	10 000
Transportation	2 000
Certification	2 000
TOTAL	**370 000**

Table 6.3: Raw costs: WP3 (Infrastructures).

Item	**Raw cost**
Lead	250 000
Clean Room	10 000
Castle Structure	45 000
Working Platform	50 000
Seismic Structure	45 000
Energy Dampers	13 000
Seismic Isolators	4 000
Travel	2 100
TOTAL	**419 100**

Table 6.4: Raw costs: WP4 (Field Cage).

Item	**Raw cost**
High Density, Radiopure Polyethylene	21 000
Oxygen Free Copper Sheets	5 000
Titanium Wire	2 500
Flanges	15 000
Casting	65 000
Casting post processing	20 000
TTX	7 000
3M foils	5 000
TPB	1 000
PTFE stock	5 000
Tefzel stock	4 000
Peek stock	4 000
HHV Cable	2 000
Machining	90 000
Travel	4 000
TOTAL	**250 500**

Table 6.5: Raw costs: WP5 (Energy plane mechanics).

Item	**Raw cost**
Copper Stock	140 000
PMT Support Plate	30 000
PMT Cans Manufacturing	60 000
Saphire Windows	110 000
Manifold Manufacturing	20 000
Fittings	7 000
Transportation	5 000
Travel	4 000
TOTAL	**376 000**

Table 6.6: Raw costs: WP6 (Energy plane sensors).

Item	**Raw cost**
Hamamatsu (R11410-10)	360 000
FEE	4 000
PMT Bases PCB	3 000
PMT Bases Components	19 000
70 channel HV power Supply	20 000
4 channel HV power Supply	4 000
External HV cables	5 000
Feedthrough	20 000
PCB	1 000
Testbed equipment	4 600
TOTAL	**440 600**

Table 6.7: Raw costs: WP7 (Tracking plane mechanics).

Item	**Raw cost**
SiPM DB support	11 000
SiPM Electronics Cu Shield	80 000
Mounting Hardware	6 000
SiPM Feedthrough	250 000
Transportation	4 000
Travel	2 000
TOTAL	**353 000**

Table 6.8: Raw costs: WP8 (Tracking plane sensors).

Item	**Raw cost**
DB cirlex	50 000
Electronic Components	2 000
SiPM	90 000
Connectors/Cabling	60 000
Trasportation	1 000
TOTAL	**203 000**

Table 6.9: Raw costs: WP9 (Tracking Front-End electronics).

Item	**Raw cost**
Front end Boards Components	96 000
FEB PCB production	15 000
FEB Component mounting	14 000
19" Eurocard chassis x 6 units	1 200
Fan trays x 6 units	2 100
Quad output 10A supplies x 6 units	12 000
CAT7 cables x 60 units	3 300
18 AWG power cabling 350 m	1 400
Front panels for FEB x 64	1 300
80 pin in vessel kapton cable x 120 units	72 000
Transportation	1 200
Travel	1 000
TOTAL	**220 500**

infrastructures can in principle be used by any experiment, and NEXT simply borrows them. The same arguments are extended to the lead castle. In any case, the help of LSC with infrastructures is essential for NEXT.

- The costs for WP4 (field cage) are fully covered by our USA collaborators.
- The costs for WP5 (energy plane mechanics) require new funds.
- The costs for WP6 (energy plane sensors) are fully covered by CUP.
- The costs for WP7 (tracking plane mechanics) require new funds.
- The costs for WP8 (tracking plane sensors) are fully covered by CUP.
- The costs for WP9 (tracking plane electronics) require new funds.
- The costs for WP10, WP11, WP12 (DAQ, computing, slow controls) require new funds.
- The costs for WP13 (radiopurity) are fully covered by CUP.
- The costs for WP14 (calibration) require new funds.

Table 6.18 shows the sharing of the costs between the different sources of funding available for the project. Notice that some significant contributions from the USA groups such as the man-hour for engineering design are not included in the table which only

Table 6.10: Raw costs: WP10 (DAQ).

Item	**Raw cost**
FECs ATCA Virtex-6	30 000
CDTC16	7 200
ADC Cards	8 000
SFP Modules - GbE	2 080
GbE CAT6 cables for PCs and FEC-to-FEC	500
PCs (LDC)	18 000
PCs (GDC)	12 000
APC Smart-UPS 5000VA 230V Rackmount/Tower	6 200
Swicth 1GbE Cisco Catalyst	3 000
Rack for PCs	2 000
PowerEdge R720	3 894
PV TL4000 LTO5-140 6Gb SAS 2 Drives	13 543
PowerEdge R620 x8 Base	10 528
PV MD3600i externo RAID iSCSI de 10Gb	10 740
PowerVault MD1200 base	11 890
PowerVault NX3610 Chassis, 10G	3 805
PowerVault NX3610 Controller, 10G	4 850
PowerConnect 8024 10GbE Managed L3 Switch	18 460
TOTAL	**166 690**

Table 6.11: Raw costs: WP11 (Offline).

Item	**Raw cost**
Dell PowerEdge M610 Blade (10)	60 000
Iomega StorCenter ix12 (10 x 20 TB)	70 000
Software	10 000
TOTAL	**140 000**

Table 6.12: Raw costs: WP12 (Slow control).

Item	**Raw cost**
Controlling PCs	10 000
Sensors (pressure, temp)	25 000
Software	10 000
Flow sensors	7 000
Integration module	10 000
TOTAL	**62 000**

Table 6.13: Raw costs: WP13 (Radiopurity)

Item	**Raw cost**
Purchase of samples	10 000
TOTAL	**10 000**

Table 6.14: Raw costs: WP14 (Calibration).

Item	**Raw cost**
Sources	6 000
Source Dropper	10 000
Control module	3 000
Travel	2 500
TOTAL	**21 500**

Table 6.15: Total raw costs.

WP 1: Vessel	521 000
WP2: Gas System	370 000
WP3: Infrastructure	419 100
WP4: Field Cage	250 500
WP5: Energy Plane Mechanics	376 000
WP6: Energy Plane Sensors	440 600
WP7: Tracking Plane Mechanics	353 000
WP8: Tracking Plane Sensors	203 000
WP9: Tracking Plane FEE	94 300
WP10: DAQ	166 690
WP11: Offline	140 000
WP12: Slow Control	62 000
WP13: Radio Purity	10 000
WP14: Calibration	21 500
TOTAL	3 553 890

Table 6.16: Raw costs status: WP1.

Item	**Paid**	**Not paid**
316Ti Stock	80 000	0
Vessel Manufacture	45 000	0
Copper Stock	0	350 000
Shield Manufacture	0	40 000
Transportation	0	2 000
Certification	0	4 000
TOTAL	**125 000**	**396 000**

Table 6.17: Raw costs status: WP2.

Item	**Paid**	**Not paid**
Purification Loop	49 000	0
Cold Getters	19 000	0
Re-circulation Compressor	0	120 000
Hot Getter	0	80 000
Cold Traps	0	15 000
Rn Trap	0	10 000
Emergency Vent Tank	0	19 000
Multi Channel RGA	0	17 000
Turbo Vacuum system	0	20 000
Rough Vacuum pump	0	7 000
25bar 100mm ID valve	0	10 000
Transportation	2 000	0
Certification	2 000	0
TOTAL	**72 000**	**298 000**

Table 6.18: Cost Sharing.

WP	USA	LSC	CUP	New Funds
WP1			125 000	396 000
WP2			72 000	298 000
WP3		419 100		
WP4	250 500			
WP5				376 000
WP6			440 600	
WP7				353 000
WP8			203 000	
WP9				220 500
WP10				166 690
WP11				140 000
WP12				62 000
WP13			10 000	
WP14				21 500
Total	250 500	419 100	850 600	2 033 690

refers to material costs. As it can be seen, existing CUP funds allow to contribute with € 850 600 to NEXT construction items. LSC funds could cover € 419 100 and the USA group will contribute with € 250 500. The raw costs not covered by existing funds adds up to € 2 033 690. Allowing for 20% taxes and 20% contingency one comes up with € 2 928 510 direct costs needed to complete the detector.

6.3 Personnel

The R&D, construction, and commissioning of the NEXT-100 detector, requires a minimum critical mass of very specialised personnel. Specifically, one needs:

1. Senior physicists, occupying top-responsibility jobs (such as the spokesperson, the project manager, the technical coordinator, etc.). Those should be permanent or semi-permanent positions. In Table 6.19 one contract is foreseen, assuming that the current R&C position hold by the software convener could be converted to permanent.

2. Senior engineers in charge of designing, constructing and maintaining the detector. At least a few of those positions should be permanent, semi-permanent or long-term contracts.

3. Post-docs and junior engineers. Ideally, those should have 3 to 5 years contracts, to exploit the expertise acquired. In Table 6.19 we foresee three postdoc positions, assuming that other three positions could be covered through contracts such as Marie Curie fellowships, R&C or Juan de la Cierva grants...

4. Electronics and mechanical technicians, with mid- to long-term contracts.

5. Graduate students, with fellowships or contracts to complete a Ph.D. (typically 5 years). In Table 6.19 we plan 5 graduate students, assuming that other 5 contracts could come from FPI/FPU/JAE fellowships.

6.3.1 Personnel cost per year

CUP funds will fully cover personnel costs until the end of the grant (December 2014), which is also the date foreseen to complete detector construction. Commissioning and operating the NEXT experiment will require at least five years.

Our current estimation of the positions needed after 2015 (excluding permanent positions) is as follows.

1. **Two senior physicists at IFIC**. Ideally, those positions should be permanent, but we budget here long-term contracts, in view of the scarcity of permanent positions foreseen for the immediate future, in particular at CSIC. The two key positions for the project that require continuity are that of: 1) technical coordinator/project manager, which is currently held by Dr. I. Liubarsky, and 2) position of software

Table 6.19: Foreseen personnel costs (all national groups in NEXT).

Cost Category	number of contracts	salary (euros)	total (euros)
Senior physicist	1	50 000	50 000
Engineers	4	35 000	140 000
post-docs	3	40 000	120 000
technicians	2	25 000	50 000
students	5	20 000	100 000
Total Personnel			460 000

Table 6.20: Personnel costs foreseen at IFIC.

Cost Category	number of contracts	salary (euros)	total (euros)
Senior physicist	1	50 000	50 000
Engineers	2	35 000	70 000
post-docs	2	40 000	80 000
technicians	2	25 000	50 000
students	3	20 000	60 000
Total Personnel			310 000

and physics coordinator, held by Dr. M. Sorel. Both of them are senior physicists at IFIC. Liubarsky has a CUP contract and Sorel has an R&D contract (he is in the last year of his contract). *Both positions are essential for the development of the experiment, and we have no replacement for the expertise and acquired knowledge of Liubarsky and Sorel, both of them top-class physicists.*

2. Four engineers (two at IFIC, two at UPV+UdG). IFIC coordinates the construction of the pressure vessel, energy plane and tracking plane as well as the front-end electronics of the PMTs and the in-vessel electronics for the SiPMs (cabling and Dice Board constructions). Currently, there are two senior engineers (one mechanical and one electronics) and two junior engineers working in the above tasks. Once the bulk of design and construction is over, one can reduce the number to one mechanical engineer and one electronics engineer, which are still needed for integration, maintenance and improvement of the systems. At UPV we have two senior electronics engineers with permanent positions, and need one expert in DAQ with a long-term contract, for development and maintenance. At UdG, we have a senior mechanical designer for the infrastructures, and need a long-term contract for maintenance of the various subsystems.

3. Four technicians (one mechanical at IFIC, one electronics at IFIC, one electronics at UdG, one at UNIZAR).

4. Eight postdocs (4 at IFIC, 2 at UNIZAR, 1 at UAM, 1 at USC). The role of the post-docs is essential, to acquire the data, run the detector, analyse the results, etc.

5. Ten graduate students (5 at IFIC, 3 at UNIZAR, 1 at UAM, 1 at USC).

Table 6.19 shows the personnel costs, which add up to € 460 000 a year for all the national groups together. The yearly costs of personnel at IFIC amounts to € 310 000.

Clearly personnel costs are high, but one has to evaluate them in the framework of the novelty, speed of development and success of the NEXT project. As discussed in Chapter 7, the IFIC group has almost no permanent positions associated with NEXT, in spite of the tremendous scientific impact of the project and its importance for the development of experimental underground physics in Spain. This situation is to be compared with the number of permanent positions (well in excess of 20) associated to the experimental groups working in collider projects (e.g., at LHC). Those groups have benefited from a well targeted policy that has allowed them to grow in a spectacular way over the last 10 years, not only at IFIC, but elsewhere in Spain. The NEXT project will need, ultimately, of a similar policy, which provides a number of key positions for senior physicists and engineers as well as the needed temporary positions (students and post-docs).

6.4 Travel and deployment at LSC

During the first five years of the NEXT project, most of the activity has taken place at the laboratories developing the prototypes. With the construction and operation

of the detector, the activity will shift heavily to the LSC. We estimate that a team of about 5 physicists, engineers and technicians from national institutions (plus about the same number from international institutions) will be permanently or semipermanently deployed at LSC. Assuming an allowance between € 30 and 40 a day (meals plus lodging) we estimate € 1 000 per person and month. Assuming 10 months deployment a year, this translates in about € 50 000 for all national groups. Additional travel (meetings, conferences, etc) is assumed to come from other sources of funding and is not contemplated in this report.

6.5 Total costs

To summarise:

1. *Costs to complete detector construction*: € 2 928 510.
2. *Personnel costs*: € 460 000 a year for all the national groups together, € 310 000 at IFIC.
3. Travel and deployment at LSC: € 50 000 a year.

Chapter 7

NEXT and CUP

7.1 Introduction

The grant allocated to CUP by the Science Ministry (MINECO) was € 5 million (direct costs). The coordinating institution is IFIC. CSIC is the managing institution, and, as such, charges overheads to the project (€ 400 000). On the other hand, CSIC has committed € 1 000 000 to CUP. Therefore, the net funds available for CUP are € 5 600 000. MINECO funds (€ 460 000) are distributed in 5 years, 2009 to 2013. CSIC funds are retained by the coordinating institution.

CUP funds are shared yearly among the participants in the consortium. The amount distributed to each institution has been negotiated on a year-by-year basis, reflecting the involvement of each group in the project, as well as its needs in personnel and equipment. Notice that CUP funds also finance the CAFE activity. Funds are distributed in 5 years, 2009 to 2013.

To understand the investment of CUP funds is important to realise that the main goal of the project was to create the infrastructures, know-how and expertise that would make it possible to develop a successful program of underground physics at the LSC. In 2009 there was no experience in the country concerning the development of high-pressure noble gas chambers. Furthermore, although the electroluminescent principle had been well known for decades, all the chambers built before NEXT-DEMO (for example in Coimbra, one of the groups participating in NEXT) were very small and not appropriated to demonstrate, at the required scale, the sophisticated EL technology needed for NEXT.

Consequently, CUP funds (€ 5 600 000) has been invested in:

1. **Supporting the CAFE activity**.
2. **Financing the R&D program (RDP)**, which extended from 2009 to 2011 and resulted in the CDR and TDR. This includes equipping laboratories, paying the construction of the prototypes and paying personnel.
3. **Purchasing equipment for the Stage I construction of the NEXT detector**. This includes all the items described in the previous chapter.

Table 7.1: Distribution of CUP funds per concept.

Concept	share (€)	% grant
CAFE	297 170	5.3
RDP (2009–2011)	2 931 708	52.4
Stage I construction (2012–2013)	850 600	15.2
Stage I personnel (2012–2013)	1 031 433	18.4
Totals	5 110 911	91.3

4. **Personnel for the Stage I construction of the NEXT detector**. This includes the salaries of senior physicists, engineers, post-docs, technicians and students during the second phase of the project.

Table 7.1 shows an estimation of the allocation of funds to the different concepts described above. This is computed as follows:

1. **Funds allocated to CAFE**. The main group in CAFE is UB, whose share of the project is € 179 050. IFIC and IFT are the other two relevant institutions in CAFE. IFIC hired a post-doc during two and a half year for CAFE activities (€ 94 570). IFT received a total of € 23 550 for CAFE activities. Thus, the total investment in CAFE adds up to € 297 170 or 5.3% of the funds.

2. **Financing the RDP (3 years)**. The funds allocated to IFAE (€ 268 250), CIEMAT (€ 234 700) and UNIZAR (€ 658 581) have been invested exclusively in the RDP. The funds allocated during the first three years of CUP to IFIC (€ 1 391 502) and UPV (€ 378 675) were also invested in the RDP, leading to the construction, commissioning and successful operation of the large NEXT-DEMO prototype, as well as the development of the prototype electronics for NEXT-100. Adding up the above figures one finds € 2 931 708 or about 52.4% of the grant.

3. **Purchasing equipment for the Stage I construction of the NEXT detector**. As described in the previous chapter, a total of € 850 600 have already been invested in equipment for NEXT-100. This includes the whole assignation of UG, which reverted to the general project. About 15.2% of CUP funds have already been invested in NEXT-100 construction.

4. **Personnel for the Stage I construction of the NEXT detector (2012-2013)**. This corresponds to the personnel allocated to IFIC (the largest group in CUP) in 2012 and 2013 (€ 781 433) as well as the personnel at UPV+ UdG (€ 160 000), IFT (€ 60 000) and USC (€ 30 000). In total, the costs of personnel during the Stage I construction of the NEXT detector adds to € 1 031 433 or 18.4% of the available funds.

The money already committed amounts, therefore, to € 5 110 911, or 91.3% of the project. The remaining ∼ € 500 000 (11% of the grant) will be invested during 2014, along with the MINECO funds allocated to NEXT in the 2013 call (project FPA2009-13697-C01, C03, and C04), which amount to € 460 000 and are distributed between IFIC and UPV.

Clearly, with the funds allocated to CUP it was not possible to finance the aggressive scientific project targeted to build the hitherto non existing expertise, demonstrate the technology with large scale prototypes, pay the specialised personnel, build up research groups *and* fully finance the NEXT-100 apparatus. In fact, the CUP project requested in its Technical Report (CTR) to the CONSOLIDER program a total of € 7 577 800. Adding 20% overhead (indirect costs) to this amount one finds € 9 093 360. Subtracting from this amount the grant which was actually allowed to CUP (€ 5 600 000) one finds € 3 493 360. The costs estimated to complete the construction of the detector are € 2 928 510 (see Chapter 6).

7.2 Funding profile (2013 & 2014)

As discussed in previous sections, about 90% of the CUP grant has already been invested. The remaining ∼ € 500 000 plus the MINECO funds allocated to the project in 2013 (€ 460 000) amount to ∼ € 960 000. The project ends nominally at the end of 2014, but we foresee asking for an extension of 6–12 months, given the current uncertainty in the research program sponsored by the ministry.

In any case, and as already discussed, personnel costs in 2014 will amount to about half of the remaining funds, with the other half allocated to operation. Discounting travel and deployment at Canfranc, that we expect to be more important in 2014 than in the previous year, we expect to allocate about € 400 000 additional to detector construction.

7.3 Needed funding

The total costs associated to the NEXT project can be estimated by adding the remaining construction costs and the operation (including personnel costs). Subtracting the € 400 000 that we expect to invest in construction from CUP funds, we can estimate the total costs to complete the construction of the NEXT-100 detector and exploit it, as follows.

1. Costs to complete detector construction: € 2 928 510.
2. Personnel costs: € 460 000 a year.
3. Travel and deployment at LSC: € 50 000 a year.
4. General operation: € 50 000 a year.

These are total direct costs, including contingency and taxes but not overheads. The costs can be spread among several participating institutions, ideally by means of an umbrella program such CUP, although a coordinated project to MINECO can also be a satisfactory solution. For NEXT-100 to be fully competitive, the detector should be built as soon as possible, and therefore one should need the construction funds to be available as soon as possible. Assuming a 3 year coordinated project, the direct costs for all groups would be € 4 608 510.

Construction costs can be reduced if we succeed in attracting international funding. On the other hand, while we have succeeded in attracting international scientific collaboration, obtaining direct funds from abroad is very hard. The main difficulty arises from the fact that there are competing experiments in USA (EXO), Japan (KamLAND-Zen), France (SuperNemo) and Italy (GERDA, CUORE). All those experiments have started, in average, ten years before NEXT, and are very well established. Many of them are also largely financed by the hosting country (e.g., USA runs with most of the costs of EXO, Japan with KamLAND-Zen, etc.).

Attracting international funding for NEXT-100 is possible, and in fact a modest but significant fraction of the detector costs will come from abroad. However, it will be much easier to convince international funding agencies to invest in NEXT (thus in LSC and in Spanish science) if and when the NEXT-100 experiment proves successful. This would open the door to a future, larger, fully internationally financed collaboration for the eventual ton scale.

Personnel costs can be reduced if the IFIC group could get one or two needed positions and a solid program of student fellowships.

7.4 Conclusions

CUP has provided the essential kick-off funds to develop the expertise, create the infrastructures, build the scientific team and launch a major scientific project. The NEXT-100 experiment at LSC has a large discovery potential, and the capability to produce first-class science at the Canfranc laboratory.

The success of the project, so far, cannot be questioned. The laboratories at IFIC and UNIZAR are now among the best of the world in the advanced technology of high-pressure chambers, and, in particular, NEXT-DEMO is the first large-scale HPXe using the EL technology. The innovations include the use of SiPM for the tracking plane, a technology that was in its infancy only five years ago. The group of the UPV is now a leader in SiPM electronics, a technology with numerous spinoffs.

The collaboration has published results that show the excellent physics case and demonstrate the good performance of the EL technology. Very good energy resolution has been measured and the topological signature of electrons has been clearly stablished.

Last but not least, an international collaboration with Spanish leadership has been created.

The next step for the project is the construction of the NEXT-100 detector. This requires new funding that match the effort already made. The funding from CUP and the

current MINECO projects finish at the end of 2014. The detector construction could be completed, the experimental teams could be kept and the experiment could be launched if a funding profile similar to that of CUP (€ 5.5 million in 5 years) could be allocated to the project, either funding the individual groups or, preferably, through an umbrella project like CUP.

The scientific opportunity is extraordinary and the ratio costs to scientific impact is relatively modest. In addition to the first-class science, NEXT would be the spring board for a future, large scale european experiment that could be run at the LSC (and financed through a large international collaboration), boosting the significance of Spain in the scientific European landscape.

Bibliography

[1] P. Hernández, *Neutrino physics*, arXiv:1010.4131.

[2] H. Klapdor-Kleingrothaus, A. Dietz, L. Baudis, G. Heusser, I. Krivosheina, et al., *Latest results from the Heidelberg-Moscow double beta decay experiment*, *Eur. Phys. J. A* **12** (2001) 147–154, [hep-ph/0103062].

[3] H. Klapdor-Kleingrothaus, A. Dietz, H. Harney, and I. Krivosheina, *Evidence for neutrinoless double beta decay*, *Mod. Phys. Lett. A* **16** (2001) 2409–2420, [hep-ph/0201231].

[4] J. J. Gomez-Cadenas, J. Martin-Albo, M. Sorel, P. Ferrario, F. Monrabal, et al., *Sense and sensitivity of double beta decay experiments*, *JCAP* **1106** (2011) 007, [arXiv:1010.5112].

[5] J. J. Gómez-Cadenas, J. Martin-Albo, M. Mezzetto, F. Monrabal, and M. Sorel, *The search for neutrinoless double beta decay*, *Riv. Nuovo Cim.* **35** (2012) 29–98, [arXiv:1109.5515].

[6] O. Cremonesi, *Experimental searches of neutrinoless double beta decay*, arXiv:1212.4885.

[7] X. Sarazin, *Review of double beta experiments*, arXiv:1210.7666.

[8] K. Zuber, *Neutrinoless double beta decay experiments*, *Acta Phys. Polon.* **B37** (2006) 1905–1921, [nucl-ex/0610007].

[9] C. M. Cattadori, *GERDA status report: Results from commissioning*, *J. Phys. Conf. Ser.* **375** (2012) 042008.

[10] J. Wilkerson, E. Aguayo, F. Avignone, H. Back, A. Barabash, et al., *The MAJORANA demonstrator: A search for neutrinoless double-beta decay of germanium-76*, *J. Phys. Conf. Ser.* **375** (2012) 042010.

[11] **CUORE** Collaboration, P. Gorla, *The CUORE experiment: Status and prospects*, *J. Phys. Conf. Ser.* **375** (2012) 042013.

[12] M. Auger, D. Auty, P. Barbeau, L. Bartoszek, E. Baussan, et al., *The EXO-200 detector, part I: Detector design and construction*, *JINST* **7** (2012) P05010, [arXiv:1202.2192].

[13] **KamLAND-Zen** Collaboration, A. Gando et al., *First result from KamLAND-Zen: Double beta decay with ^{136}Xe*, arXiv:1205.6130.

[14] **NEXT** Collaboration, V. Alvarez et al., *NEXT-100 Technical Design Report (TDR): Executive Summary*, *JINST* **7** (2012) T06001, [arXiv:1202.0721].

[15] **KamLAND-Zen** Collaboration, A. Gando et al., *Measurement of the double-β decay half-life of ^{136}Xe with the KamLAND-Zen experiment*, *Phys. Rev. C* **85** (2012) 045504, [arXiv:1201.4664].

[16] **EXO** Collaboration, N. Ackerman et al., *Observation of Two-Neutrino Double-Beta Decay in ^{136}Xe with EXO-200*, *Phys. Rev. Lett.* **107** (2011) 212501, [arXiv:1108.4193].

[17] **KamLAND** Collaboration, S. Abe et al., *Production of Radioactive Isotopes through Cosmic Muon Spallation in KamLAND*, *Phys.Rev.* **C81** (2010) 025807, [arXiv:0907.0066].

[18] **KamLAND-Zen** Collaboration, A. Gando et al., *Limit on Neutrinoless $\beta\beta$ Decay of Xe-136 from the First Phase of KamLAND-Zen and Comparison with the Positive Claim in Ge-76*, arXiv:1211.3863.

[19] **EXO** Collaboration, E. Conti et al., *Correlated fluctuations between luminescence and ionization in liquid xenon*, *Phys. Rev. B* **68** (2003) 054201, [hep-ex/0303008].

[20] **EXO** Collaboration, M. Auger et al., *Search for Neutrinoless Double-Beta Decay in ^{136}Xe with EXO-200*, *Phys.Rev.Lett.* **109** (2012) 032505, [arXiv:1205.5608].

[21] J. Bergstrom, *Combining and comparing neutrinoless double beta decay experiments using different nuclei*, arXiv:1212.4484.

[22] N. Haba and R. Takahashi, *Constraints on neutrino mass ordering and degeneracy from Planck and neutrino-less double beta decay*, arXiv:1305.0147.

[23] **Planck Collaboration** Collaboration, P. Ade et al., *Planck 2013 results. XVI. Cosmological parameters*, arXiv:1303.5076.

[24] **NEXT** Collaboration, V. Álvarez et al., *Initial results of NEXT-DEMO, a large-scale prototype of the NEXT-100 experiment*, arXiv:1211.4838.

[25] **NEXT** Collaboration, J. Martín-Albo and J. J. Gómez-Cadenas, *Status and physics potential of NEXT-100*, arXiv:1301.2966.

[26] J. Gomez-Cadenas, J. Martin-Albo, J. Munoz-Vidal, and C. Pena-Garay, *Discovery potential of xenon-based neutrinoless double beta decay experiments in light of small angular scale CMB observations*, arXiv:1301.2901.

[27] **Caltech-Neuchâtel-PSI** Collaboration, R. Luscher et al., *Search for $\beta\beta$ decay in Xe-136: New results from the Gotthard experiment*, *Phys. Lett. B* **434** (1998) 407–414.

[28] D. Nygren, *High-pressure xenon gas electroluminescent TPC for 0nu beta beta-decay search*, *Nucl.Instrum.Meth.* **A603** (2009) 337–348.

[29] **NEXT** Collaboration, V. Alvarez et al., *The NEXT-100 experiment for neutrinoless double beta decay searches (Conceptual Design Report)*, arXiv:1106.3630.

[30] V. Alvarez et al., *Radiopurity control in the NEXT-100 double beta decay experiment: procedures and initial measurements*, arXiv:1211.3961.

[31] K. Lung, K. Arisaka, A. Bargetzi, P. Beltrame, A. Cahill, T. Genma, C. Ghag, D. Gordon, J. Sainz, A. Teymourian, and Y. Yoshizawa, *Characterization of the Hamamatsu R11410-10 3-in. photomultiplier tube for liquid xenon dark matter direct detection experiments*, *Nuclear Instruments and Methods in Physics Research A* **696** (Dec., 2012) 32–39, [arXiv:1202.2628].

[32] **NEXT** Collaboration, V. Alvarez et al., *Near-Intrinsic Energy Resolution for 30 to 662 keV Gamma Rays in a High Pressure Xenon Electroluminescent TPC*, arXiv:1211.4474.

[33] **NEXT** Collaboration, V. Álvarez et al., *Ionization and scintillation response of high-pressure xenon gas to alpha particles*, arXiv:1211.4508.

[34] C. Silva, J. Pinto da Cunha, A. Pereira, V. Chepel, M. Lopes, et al., *Reflectance of Polytetrafluoroethylene (PTFE) for Xenon Scintillation Light*, arXiv:0910.1056.

[35] **NEXT** Collaboration, V. Alvarez et al., *Initial results of NEXT-DEMO, a large-scale prototype of the NEXT-100 experiment*, *JINST* **8** (2013) P04002, [arXiv:1211.4838].